ISTANBUL TECHNICAL UNIVERSITY ★ GRADUATE SCHOOL OF SCIENCE ENGINEERING AND TECHNOLOGY

SYNTHESIS & CHARACTERIZATION OF CdSe/ZnS QUANTUM DOTS

M.Sc. THESIS

Hakan AYDIN

Department of Nanoscience & Nanoengineering

Nanoscience & Nanoengineering Programme

MAY 2014

ISTANBUL TECHNICAL UNIVERSITY ★ GRADUATE SCHOOL OF SCIENCE ENGINEERING AND TECHNOLOGY

SYNTHESIS & CHARACTERIZATION OF CdSe/ZnS QUANTUM DOTS

M.Sc. THESIS

Hakan AYDIN
(513111007)

Department of Nanoscience & Nanoengineering

Nanoscience & Nanoengineering Programme

Thesis Advisor: Prof. Dr. Hilmi ÜNLÜ

MAY 2014

İSTANBUL TEKNİK ÜNİVERSİTESİ ★ FEN BİLİMLERİ ENSTİTÜSÜ

CdSe/ZnS KUANTUM NOKTALARININ SENTEZİ VE KARAKTERİZASYONU

YÜKSEK LİSANS TEZİ

Hakan AYDIN
(513111007)

Nanobilim ve Nanomühendislik Anabilim Dalı

Nanobilim ve Nanomühendislik Programı

Tez Danışmanı: Prof. Dr. Hilmi ÜNLÜ

MAYIS 2014

Hakan AYDIN, a **M.Sc.** student of ITU **Graduate School of Science Engineering and Technology** student ID 513111007, successfully defended the **thesis** entitled "**SYNTHESIS AND CHARACTERIZATION OF CdSe/ZnS QUANTUM DOTS**", which he prepared after fulfilling the requirements specified in the associated legislations, before the jury whose signatures are below.

Thesis Advisor :	**Prof. Dr. Hilmi ÜNLÜ** İstanbul Technical University	.....
Jury Members :	**Prof. Dr. Hikmet YÜKSELİCİ** Yıldız Technical University	.....
	Assoc. Prof. Esra ÖZKAN ZAYİM İstanbul Technical University	.....

Date of Submission : 05 May 2014
Date of Defense : 30 May 2014

To my children won't be born,

FOREWORD

I would firstly like to thank my advisor, Prof. Dr. Hilmi ÜNLÜ for his contributions and leading me to complete my study on the way of success.
I would like to thank Mesut BALABAN, for spending most of his time in our laboratory and discussing the difficulties i have been faced to find the right way. He also showed me how to take carefully the synthesis procedure of nanoparticles.
I would like to thank research assistants Aytül FİLİZ, Nesrin ATMACA ÇELEBİOĞLU, Ramazan ŞAHİN, Sevcan TABANLI and proficient Tansu ERSOY for their helps without any benefits within the Department of Physics. I could not handle the situations in physics labrotary for engineer candidates and photoluminescence study of nanocrystals without Nesrin ATMACA and Sevcan TABANLI's help.
Without any doubt, i have to thank special people Tuğçe TUNCA, who motivates me to stay in the game and avoid me to give up.
I would also like to thank my family, as they have always backed up me to overcome the difficulties and approcahed patiently during my education period.

May 2014

Hakan AYDIN
(Physicist)

TABLE OF CONTENTS

Page

FOREWORD ..... **viii**
TABLE OF CONTENTS ..... **xi**
ABBREVIATIONS ..... **xiii**
LIST OF TABLES ..... **xv**
LIST OF FIGURES ..... **xvii**
SUMMARY ..... **xix**
ÖZET ..... **xxiii**
1. INTRODUCTION **1**
1.1 Quantum Dots (QDs) 1
1.1.1 The structure of QDs 2
1.1.1.1 Basic quantum mechanics & energy band modelling 3
1.1.1.2 Core-shell QDs & heterojunctions 6
1.1.2 Optical properties of QDs 8
2. SYNTHESIS **11**
2.1 Experimental Study 13
2.1.1 Synthesis of CdSe core QDs 13
2.1.2 Growth of ZnS shells on CdSe core QDs 14
3. CHARACTERIZATION **17**
3.1 Optical Characterization of CdSe & CdSe/ZnS QDs 17
3.2 Photoluminescence of CdSe & CdSe/ZnS QDs 21
3.3 Morphological Analysis & Determination of NC Diameter 24
4. RESULTS & DISCUSSION **29**
4.1 Effect of Temperature & Precursor Ratio on the NC Growth 29
4.2 Emission Quality & Photoluminescence Quantum Yield of NCs 31
5. CONCLUSION **35**
REFERENCES **37**
CURRICULUM VITAE **41**

ABBREVIATIONS

AFM	**:** Atomic Force Microscopy
CB	**:** Conduction Band
Cd	**:** Cadmium
CdO	**:** Cadmium Oxide
CdS	**:** Cadmium Sulfide
CdSe	**:** Cadmium Selenide
CdTe	**:** Cadmium Telluride
FWHM	**:** Full Width at Half Maximum
HRTEM	**:** High Resolution Transmission Electron Microscopy
LED	**:** Light Emitting Diode
N_2	**:** Nitrogen
NC	**:** Nanocrystal
PL	**:** Photoluminescence
QD	**:** Quantum Dot
QY	**:** Quantum Yield
S	**:** Sulfide
Se	**:** Selenium
Te	**:** Tellurium
TOP	**:** Trioctylphosphine
VB	**:** Valence Band
XRD	**:** X-Ray Diffraction
Zn	**:** Zinc
$Zn(OAc)_2.2H_2O$	**:** Zinc Acetate Dihydrate
ZnS	**:** Zinc Sulfide

LIST OF TABLES

Page

Table 4.1 : Effect of Cd:Se initial precursor ratio on the FWHM values of CdSe NCs..... 31
Table 4.2 : PL properties of CdSe QDs grown at 160°C with Cd:Se ratio of 1:1.25 and CdSe/ZnS QDs deposited over with number of cycles. 33
Table 4.3 : PL properties of CdSe QDs grown at 170°C with Cd:Se ratio of 2:1 and CdSe/ZnS QDs deposited over within one cycle for given time intervals. 33

LIST OF FIGURES

Page

Figure 1.1 : Density of states of a a) bulk material, b) quantum well, c) quantum wire and d) quantum dot. 2
Figure 1.2 : Band gap of QDs with different sizes in comparison to bulk form. 3
Figure 1.3 : Energy dispersion relationship for a free particle. 4
Figure 1.4 : Energy versus momentum dispersion of bulk solids for small values of momentum. Due to coupling effects of orbital motion around the host atom and electron spin, there are two types of holes, adapted from (Sattler,2011). 5
Figure 1.5 : Possible band structure alignment for core-shell QDs, adapted from (Sattler,2011). 7
Figure 1.6 : Band structure alignment near the interface of two different materials, adapted from (Sattler,2011). 7
Figure 1.7 : Absorption mechanism model for QDs. 10
Figure 2.1 : Energetic band positions and lattice mismatch of semiconductor CdSe/CdS and CdSe/ZnS combinations, adapted from (Xie *et al*, 2005). 12
Figure 2.2 : Typical synthesis procedure for CdSe core QDs. 14
Figure 2.3 : CdSe QDs synthesized at 160°C with Cd:Se ratio of 1:10. 14
Figure 2.4 : Typical synthesis procedure for ZnS shell growth on CdSe core NCs. 15
Figure 2.5 : CdSe core QDs (left) synthesized at 160°C with a Cd:Se ratio of 1:1.25 and CdSe/ZnS core-shell QDs (right) covered over at 145°C within 3 cycles. 15
Figure 2.6 : Layout of equipment for synthesis of CdSe and CdSe/ZnS NCs. 16
Figure 3.1 : Absorption spectra of the CdSe QDs synthesized at 160°C with Cd:Se ratio of 1:5. 17
Figure 3.2 : Absorption spectra of the CdSe QDs synthesized at 170°C with Cd:Se ratio of 1:2.5. 18
Figure 3.3 : Absorption spectra of the CdSe QDs synthesized at 160°C with Cd:Se ratio of 1:1.25. 18
Figure 3.4 : Normalized absorption spectra of CdSe – 35 mins sample synthesized at 160°C with Cd:Se ratio of 1:1.25 and CdSe/ZnS core-shell QDs grown on throughout the cycles. 19
Figure 3.5 : $(\alpha h\nu)^2$ vs. $h\nu$ plot of CdSe QDs synthesized at 160°C with Cd:Se ratio of 1:5. 20
Figure 3.6 : $(\alpha h\nu)^2$ vs. $h\nu$ plot of CdSe QDs synthesized at 170°C with Cd:Se ratio of 1:2.5. 20
Figure 3.7 : $(\alpha h\nu)^2$ vs. $h\nu$ plot of CdSe QDs synthesized at 160°C with Cd:Se ratio of 1:1.25. 21

Figure 3.8 : Normalized PL spectra of CdSe QDs synthesized at 160°C with Cd:Se ratio of 1:1.25. 23
Figure 3.9 : Normalized PL spectra of CdSe QDs synthesized at 170°C with Cd:Se ratio of 1:1.25. 23
Figure 3.10 : HRTEM image of CdSe QDs synthesized at 170°C with Cd:Se ratio of 1:5. The label is indicator of 20 nm length. The average diameter is 3±0.3 nm where the calculated value is 2.984 nm. 25
Figure 3.11 : HRTEM image of CdSe QDs synthesized at 170°C with Cd:Se ratio of 1:5. The label is indicator of 10 nm length. The average diameter is 3.1±0.2 nm where the calculated value is 2.984 nm. 25
Figure 3.12 : HRTEM image of CdSe QDs synthesized at 160°C with Cd:Se ratio of 1:2.5. The label is indicator of 100 nm. 26
Figure 3.13 : HRTEM image of CdSe QDs synthesized at 160°C with Cd:Se ratio of 1:2.5. The label is indicator of 10 nm. The average diameter is 3.1±0.2 nm where the calculated value is 2.944 nm. 26
Figure 3.14 : XRD pattern of the CdSe/ZnS core-shell QDs with Cd:Se precursor ratio of 2:1 (CdSe synthesis temperature: 170°C). Lattice planes correspond to JCPDS file No. 77-2100 for ZnS shell and JCPDS file No. 19-0191 for CdSe core. 27
Figure 4.1 : Growth of CdSe NCs with different Cd:Se molar ratios at 160°C. 29
Figure 4.2 : Effect of temperature on CdSe NCs growth for Cd:Se ratio of 1:2.5. 30
Figure 4.3 : Effect of temperature on CdSe NCs growth for Cd:Se ratio of 1:5. 30
Figure 4.4 : Effect of temperature on CdSe NCs growth for Cd:Se ratio of 1:10. 31
Figure 4.5 : Normalized PL spectra of CdSe and CdSe/ZnS NCs. 32
Figure 4.6 : PL spectra of CdSe QDs synthesized at 170°C with Cd:Se ratio of 1:1.25. 33

SYNTHESIS & CHARACTERIZATION OF CdSe/ZnS QUANTUM DOTS

SUMMARY

Owing to the increasing demands for high quality (monodispersity, high crystallinity, narrow emission spectrum and high quantum yield) NCs, it is important to develop low-cost, green and mass produceable synthesis routes. Nanocrystals (NCs) synthesized by a chemical route allow us to control their sizes and distribution. Altering the concentrations of reactants or changing the processing times at different temperatures of production may result in various properties of colloidal NCs.

Colloidal semiconductor NCs (also known as quantum dots (QDs)) with their diameters range between 2-10 nm have gained a huge interest for both optical and electronical applications such as solar cells, light emitting diodes (LEDs), lasers, fluorescence imaging and for fundamental studies over the last few decades due to their size-dependent optical, physical and chemical properties. These small-sized nanostructures have a large surface-to-volume ratio and constitute a class of materials intermediate between molecular and bulk forms of matter. QDs can be sytnhesized in core (bare) or core-shell forms due to interest and generally are made from III-V and II-VI family or semiconductors in the periodic table.

With recent advances in materials manipulation at the nanoscale, the degrees of freedom of charge carriers can be controlled to produce electron confinement in structures like QDs. Because of the strong confinement imposed in all three spatial directions, QDs behave similarly to atoms. Due to similar diameters of NCs that in the scale of De Broglie wavelength or Bohr exciton radius, size quantization effect is observed. The conduction band (CB) or the valence band (VB) is split into subbands or discrete levels depending on the dimensionality of the confined structure. As the size of NC gets smaller, the effective band gap and energy amount to be excited increases where the emission wavelength decreases. Chemically passivating the NC core with a thin shell of wide band gap semiconductor prevents chemical interaction with the inter-NC environment and provides better optical properties. Depending on the combination of materials used in the core and shell regions, it is possible to control the relation position of electrons and holes. When electrons and holes are spatially separated between core and shell, it is said that the QD exhibits type-II confinement (CdSe/CdTe QDs); otherwise, it exhibits type-I confinement (CdSe/ZnS and CdSe/CdS QDs).

Once an electron-hole pair is created by the absorption of a photon, they interact with each other by means of their opposite charges, forming a quasi-particle called “exciton”. The total energy of an exciton indicates the color (wavelength) of the light emitted by the quantum systems. The dispersion or energy versus momentum (which is proportional to the wave vector k) curves are parabolic just as for classical free particles with some modifications.

CdSe NCs, a member of the II-VI semiconductor family with a direct band gap, are mostly investigated NCs due to their bright luminescence in the visible range of optical spectrum with varying particle size. In this thesis, it was aimed that the

synthesis of both CdSe core and CdSe/ZnS core-shell NCs at relatively low temperature and characterizing the NCs by altering the temperature, time and initial Cd:Se precursor ratios.

For the synthesis of CdSe core NCs, firstly, cadmium stearate ($C_{36}H_{70}CdO_4$), the Cd precursor, is prepared by heating the mixture of CdO (0.01 mol, 1.284 g) and stearic acid ($C_{18}H_{36}O_2$) (0.02 mol, 5,68 g) at 170°C for 15 mins in order to use in further reactions. For a typical synthesis of CdSe core NCs, cadmium stearate (0.1358 g, 0.2 mmol) is added into a three-neck flask with 16 mL paraffin liquid without Se precursor as the Se can't be dissolved without any phosphine-based material at relatively lower temperatures than used in original method. To overcome this situation, 2 mL TOP and Se powder (0.0078 g, 0.1 mmol) are added into a flask and are mixed in an ultrasonic cleaner at the room temperature for several seconds. The cadmium stearate-paraffin mixture is degassed in vacuum at room temperature and then is heated to a desired temperature (160-180°C) with oil-bath heating for reaction under N_2 flow. When the heat is arised to aimed temperature, TOP-Se solution is rapidly injected into the reaction flask for the nucleation and growth of CdSe NCs.

Aliquots are taken at different time intervals via a syringe to monitor the growth of CdSe core NCs. After cooling down to room temperature, aliquots are centrifuged by addition of acetone at least three times to purify core solution. The end products are heated up to 60°C under vacuum to get rid of remaining solvents.

After collecting total 8 mL of samples by the end of CdSe core synthesis; the resulting core solution, $Zn(OAc)_2.2H_2O$ (0.085 mmol, 0.01866 g) and S powder (0.085 mmol, 0.00272 g) are mixed together in the reaction flask. The reaction volume is adjusted to 15 mL by adding paraffin liquid. Then the mixture is degaseed at 80°C for 20 mins. Afterward, reaction temperature is set to 145°C for the shell growth under N_2 atmosphere. Aliquots are taken at different time intervals to monitor the shell growth. To grow ZnS shells with different thicknesses around the CdSe core, a seeding-growth technique was adapted. By the end of each cycle, the same amount of Zn and S precursors are added into reaction flask and volume is adjusted to initial value by adding lack of paraffin liquid to complete 3 cycles until a desired core-shell NCs are obtained. The final products are precipitated by addition of acetone with a centrifuge step. After the centrifuging, aliquots are dried at 60°C under vacuum to get rid of remaining solvents for further processing.

Our investigations of the optical and electronical properties of synthesized CdSe core and CdSe/ZnS core-shell NCs are well-matched with studies in the literature. Depending on the diameter of CdSe NCs, the red shift was observed in their absorption spectra. In coherent with the situation, a decrease in the optical absorption band gap of NCs was recorded, thus proving the size quantization effect. The FWHM values of CdSe core and CdSe/ZnS core-shell NCs were found to vary between 25-31 nm without Ostwald ripening, indicating the luminescence quality of synthesized particles in narrow size distribution. For the synthesis' with altering the Cd:Se initial precursor ratio at a fixed temperature, it was observed that the samples with a high Cd:Se ratios are able to nucleate and grow faster. However, it was explored that the influence of operating temperature becomes dominant on the growth of NCs as the Cd:Se initial precursor ratio decreases. It was attributed to unfavorable temperatures for the growth of Cd rich samples. For a fixed temperature, it was investigated that there is an increase for FWHM values obtained from PL spectras by reducing the Cd:Se initial precursor ratio. The same situation is also valid for deposition of ZnS shells over CdSe core NCs. PL QY results were showed it is possible to increase the efficiency of CdSe core NCs with covering ZnS shells over them. Average particle

diameters obtained from high resolution TEM images were suitable with the derived particle diameters from theoretical calculations by using effective mass approximation.

CdSe/ZnS KUANTUM NOKTALARININ SENTEZİ & KARAKTERİZASYONU

ÖZET

Kimyasal yöntemler ile üretilen nanokristaller, bize parçacıkların boyut dağılımlarını kontrol edebilme ve ayarlayabilme ihtimâlini sunmaktadır. Üst düzey niteliklere sahip nanoparçacıklara duyulan ihtiyaç ve ilgi, gün geçtikçe artmaktadır. Bu bağlamda düşük maliyetli, çevreci ve büyük miktarda nanokristal üretimi büyük bir önem arz etmektedir.

Kimyasal üretim sürecinde sıcaklık, öncü malzemelerin molar oranları ve zaman gibi niceliklerin belirli ölçülerde değiştirilmesi, üretilen nanokristallerin farklı elektronik ve optik özelliklere sahip olmasını sağlamaktadır. Böylece, ihtiyaç duyulan özelliklere sahip nanokristalleri elde etmek adına üretim sürecinde öngörülen değişikliklere gidilebilmektedir.

Kuantum noktaları olarak da adlandırılan kolloidal yarı iletken nanokristaller, 2-10 nm arasında değişen parçacık çaplarına sahiptir ve floresans görüntüleme, ışık yayan diyotlar, düz panel görüntüleme sistemleri, güneş pilleri, lazerler ve biyolojik tedaviler gibi birçok farklı alanda uygulamalara konu olmaktadır. Yüksek yüzey-hacim oranı sayesinde nanokristaller, boyutlarına bağlı olarak değişebilen optik, elektriksel ve kimyasal özelliklerini beraberinde getirmektedir. Genellikle II-VI ve III-V periyodik grup elementlerinin birleşimi ile ortaya çıkan kuantum noktaları, moleküler ve yığınsal malzeme arasında kendilerine has bir sınıf oluşturmuştur ve çekirdek ya da çekirdek-kabuk yapılar şeklinde üretilebilmektedir.

Gelişen teknoloji ile birlikte yük taşıyıcılarının serbestlik dereceleri, elektron sınırlama özelliği oluşturabilmek adında kullanılmaktadır. Kuantum noktaları, elektronları uzaysal üç boyutta sınırlama özelliğine sahip olduklarından dolayı "boyutsuz" yapılar olarak adlandırılabilmektedir. Bu sınırlama şartlarından dolayı kuantum noktaları, atomlara benzer davranışlar sergilemektedir. Bohr-exciton yarıçapına yakın boyutlarından dolayı kuantum noktalarında "boyutu niceleme etkisi" gözlenmektedir. Böylece iletim ve değerlik bantları, alt bantlara (kesikli değerlere) bölünür. Bütün bu özellikler doğrultusunda nanokristal boyutu (çapı) küçüldükçe etkin bant aralığı artar ve gözlemlenen renkte maviye doğru kayma gözlemlenir. Kuantum noktalarında parçacık hareketini tanımlamak için tek bant etkin kütle yaklaşımı kullanılır ve hareket denklemi zamandan bağımsız Schrödünger denkleminin silindirik apsis düzeninin birinci ya da ikinci mertebeden çözümü ile elde edilir.

Nanokristal çekirdek yapının geniş bir bant aralığına sahip yarı iletken malzeme ile ince bir tabaka şeklinde kaplanıp kimyasal olarak etkisizleştirilmesi, çekirdeğin kimyasal tepkimelerden uzak tutulmasına ve optik özelliklerinin iyileşmesine yol açar. Kullanılan malzemelerin bir araya getirilme şekline göre iki farklı çekirdek-kabuk yapısı mevcuttur. Elektron ve boşlukların uzaysal olarak çekirdek ve kabuk bölgelerinde ayrı şekilde hapsedilmesi durumunda "ikinci tip sınırlama", geri kalan diğer olasılıklar için de "birinci tip sınırlama" söz konusu olur.

Nanokristaller, etkin bant aralığı enerjisine yakın bir düzeydeki enerji ile uyarıldıklarında elektron-boşluk çifti (eksiton) oluşur. Eksitonun toplam enerjisi, kuantum düzenekleri tarafından yayımlanan dalga boyunu, başka bir deyişle rengi belirler.

CdSe nanokristaller, II-VI periyodik ailesinin bir üyesi olup doğrudan bant geçişine sahip yarı iletken bir malzemedir. Parçacık boyutuna bağlı olarak değişen optik tayfın görünür bölgesindeki parlak ışıma yeteneği, CdSe nanokristalleri üzerinde en çok araştırma yapılan malzemelerden biri hâline getirmiştir. Kullanılan yöntem çerçevesinde CdSe nanokristalleri 20-300°C arasında değişen sıcaklıklarda üretmek mümkündür. 100°C ve altındaki sıcaklıklarda üretilen CdSe nanokristaller genellikle suda çözünebilir ve üretim işlemi uzun süreler alır. Üretim sıcakığı yükseldikçe ulaşılmak istenen parçacık boyutu dağılımını yakalama süresi, daha hızlı büyüme olacağından kısalır. Buna rağmen, dar bir boyut dağılımı elde etmek için nispeten düşük başlangıç sıcaklıkları kullanmakta fayda vardır.

Bu tezin kapsamında CdSe çekirdek ve CdSe/ZnS çekirdek-kabuk nanoyapıların göreceli olarak düşük sıcaklıklarda üretilmesi ve üretim sırasında çeşitli niceliklerin değiştirilmesi sonucu elde edilen kuantum noktalarının öz niteliklerinde ortaya çıkan farklılıkları gözlemlemek ve karakterize etmek amaçlanmıştır. Literatürden uygun olduğu kanısına varılarak seçilmiş inorganik tabanlı bir yöntem, laboratuar imkânları doğrultusunda ufak değişikliklere tabii tutularak uygun duruma getirilmiştir.

CdSe çekirdek nanokristalleri üretimi için öncelikle kadmiyum stearat ($C_{36}H_{70}CdO_4$), kadmiyum oksit (CdO) (0.01 mol, 1.284 g) ve stearik asitin ($C_{18}H_{36}O_2$) (0.02 mol, 5,68 g) 170°C'de 15 dakika sure ile karıştırılması ile hazırlanır. Elde edilen ürün daha sonra çoklu üretimler için öncü malzeme olarak kullanılabilir. Kadmiyum stearat (0.1358 g, 0.2 mmol) ve 16 mL likit paraffin üç boyunlu cam balon içerisine konur ve manyetik karıştırıcı vasıtasıyla 15 dakika sure boyunca vakuma alınarak oksit içerikli malzemenin içindeki havanın uzaklaştırılması sağlanır. Toz hâlindeki selenyum, nispeten düşün sıcaklıklarda kendi başına çözünemediğinden ilâve olarak trioktilfosfin (TOP) kullanılır. Selenyumun tamamen çözülmesi için bir cam balon içine 2 mL TOP ve selenyum (0.0078 g, 0.1 mmol) ilâve edildikten sonar oda sıcaklığında ultrasonic temizleyici içerisinde yaklaşık 12-13 saniyede çözülmesi sağlanır. Kadmiyum stearat ve paraffin karışımından oksijenin uzaklaştırılmasının ardından deney balonunun içine azot gazı akışı başlatılır ve arzu edilen sıcaklığa ulaşması için ısıtılır (160-180°C). Hedeflenen sıcaklığa ulaşıldığında TOP-Se çözeltisi karışıma hızlıca eklenir ve nanokristallerin çekirdeklenme evresi başlatılmış olur. TOP-Se çözeltisinin eklenmesinin hemen ardından birkaç saniye içinde gözle görülür bir renk değişimi fark edilebilir. Farklı boyutlarda CdSe nanokristallerin büyümesini gözlemlemek için deney süresince belirli aralıklarda şırınga yardımıyla 1 mL'lik örnekler toplanır. Son örnek de alındıktan sonra geri kalan malzeme, üzerine ZnS kaplanmak üzere kenara ayrılır.

Alınan örnekler, oda sıcaklığına soğuduktan sonra aseton ile santrifüj işlemi en az 3-4 kez tekrarlanarak gerçekleştirilir. Santrifüj işlemi tamamlandıktan sonra geri kalan çözücüleri uzaklaştırmak için CdSe nanokristaller vakumlu fırın içine konularak 60°C sıcaklıkta yaklaşık 10-15 dakika boyunca tutulur. Fırından alınan örneklere hekzan eklenerek optik karakterizasyona hazır duruma getirilir.

CdSe/ZnS çekirdek-kabuk yapısındaki nanokristallerin üretimi için CdSe çekirdek çözeltisinden geriye kalan yaklaşık 8 mL'lik malzeme üzerine çinko asetat dehidrat ($Zn(OAc)_2.2H_2O$) (0.085 mmol, 0.01866 g) ve toz hâlinde kükürt (S) (0.085 mmol, 0.00272 g) eklenir ve karıştırılır. Çözeltinin toplam hacmini 15 mL yapacak miktarda likit paraffin eklenir ve 80°C sıcaklıkta 20 dakika boyunca vakuma alınıp

karıştırılarak içindeki havanın tahliyesi sağlanır. Daha sonra sıcaklık 145°C olarak ayarlanır ve üretimin yapıldığı cam balon içerisine azot gazı akışı başlatılır. Farklı boyutlarda kabukların kaplanması için besleyerek büyütme yöntemi kullanılır ve CdSe çekirdek nanokristallerin üretiminde olduğu gibi belirli aralıklar ile örnekler alınır. Belirlenen sürenin sonuna gelindiğinde üretimin başında kullanılan ile aynı miktarda öncü malzemeler eklenerek istenilen kabuk kalınlığına ulaşılana kadar süreç tekrarlanır. CdSe çekirdek nanokristallerin üretiminden sonra olduğu gibi, yine aseton aracılığı ile santrifüj işlemi en az 3-4 defa olmak üzere gerçekleştirilir ve kalan çözücüleri uzaklaştırmak için örnekler 60°C sıcaklıkta vakumlu fırında 10-15 dakika süre ile bekletilir; en son hekzan ilâvesi ile optik karakterizasyona hazır duruma getirilir.

Üretilen CdSe çekirdek ve CdSe/ZnS çekirdek-kabuk nanokristallerin sahip olduğu optik ve elektronik özelliklerin literatürdeki verilerle uyumlu olduğu görülmüştür. Parçacık boyutlarına bağlı olarak üretilen CdSe çekirdek nanokristallerin soğurma tayfında artan parçacık çapı ile beraber kırmızıya kayma gözlemlenmiştir. Bu durumla bağdaşır şekilde, üretilen yarı iletken nanokristallerin optik soğurma bant aralıklarında artan parçacık boyutu ile beraber daralma kaydedilmiş ve boyutu niceleme etkisi kanıtlanmıştır. CdSe ve CdSe/ZnS nanokristallerin optik ışıldama tayflarındaki yarı yükseklikteki tam genişlik değerleri yaklaşık 25-31 nm arasında belirlenmiş ve ışıldama yeteneklerinin niteliklerinin üst düzeyde olduğu görülmüştür. Ayrıca hazırlanan örneklerin çoğunda Ostwald olgunlaşma davranışına ait belirgin izler saptanmamıştır. Sabit sıcaklıkta Cd:Se öncü malzeme oranı değiştirilerek yapılan üretimlerde Cd:Se oranının yüksek olduğu örneklerin daha hızlı büyüdüğü görülmüştür. Bununla beraber, Cd:Se oranı düştükçe sıcaklığın parçacıkların büyümesi üzerindeki etksinin arttığı görülmüştür. Bu durumun sebebi, üretim sürecinde kullanılan sıcaklıkların (160-170°C) kadmiyum açısından zengin örneklerin büyümesi için düşük kalması olarak açıklanmıştır. Sabit sıcaklıkta Cd:Se oranı değiştirilerek üretilen örneklerden gözlemlenen diğer bir özellik de selenyum miktarının artmasıyla beraber ışıldama tayfından ölçülen yarı yükseklikteki tam genişlik değerlerinin artmasıdır. Aynı durum, CdSe çekirdek nanokristaller üzerine kaplanan ZnS kabuk kalınlığının artmasıyla da gözlemlenmiştir. ZnS kabukların kaplandığına dair kanıt, soğurma tayfında gözlemlenen kırmızıya kayma eğilimi olarak gösterilmiş ve literatür ile tutarlı olduğu görülmüştür. Üretilen nanokristallerin kuantum verimi hesaplanmış ve ZnS kabuk kaplamanın CdSe çekirdek nanokristallerin kuantum verimini arttırabildiği kanıtlanmıştır. Yüksek çözünürlüklü TEM görüntülerinden elde edilen parçacık çapları ile etkin kütle yaklaşımı kullanarak teorik olarak hesaplanan boyutların birbiri ile tutarlı olduğu görülmüştür.

1. INTRODUCTION

The current demand of the world for energy supply and consuming habits of people in the frame of "always having the better one" push the scientists to search for effective routes to build devices or materials that are smaller, faster, compatible and can supply sustainable energy. To relieve the energy crisis and utilize the devices based on energy conversion/storage (solar cells, batteries, thermoelectrics etc.), sensors (gas sensors, photovoltaics etc.) and catalysis covering photodegradatiton of toxic dyes and catalytic oxidation of carbon monoxide in the atomic scale, researchers have focused on semiconductor nanocrystal-based applications.

Nanocrystals (NCs) synthesized by a chemical route allow us to control their sizes and distribution. These routes include single molecule precursor, sonochemistry, solvothermal synthesis, microwave irradiation, organometallic precursor route and green chemical applications. Owing to increasing demands for high quality (monodispersity, high crystallinity, narrow emission spectrum and high quantum yield) NCs, it is important to develop low-cost, green and mass produceable synthesis routes.

Altering the concentrations of reactants or changing the operating times at different temperatures of production may result in various properties of colloidal NCs. For example, it is possible to synthesize differently sized CdSe NCs that emit from blue to red color by tuning the parameters cleverly during the reaction stage in order to use for different applications.

1.1 Quantum Dots (QDs)

Colloidal semiconductor NCs (also known as quantum dots (QDs)) with their diameters range between 2-10 nm have gained a huge interest for both optical and electronical applications such as solar cells [1-4], light emitting diodes (LEDs) [5-7], lasers [8, 9] and for fundamental studies [10-14] over the last few decades due to their size-dependent optical, physical and chemical properties. These small-sized

nanostructures have a large surface-to-volume ratio and constitute a class of materials intermediate between molecular and bulk forms of matter. QDs can be sytnhesized in core (bare) or core-shell forms due to interest.

QD NCs are composed of chemical elements in the periodic groups II-VI, III-V, or IV-IV. A QD can obtain single electron to several thousands of electrons since the size of QD is designable.

1.1.1 The structure of QDs

With recent advances in materials manipulation at the nanoscale, the degrees of freedom of charge carriers can be controlled to produce electron confinement in structures like QDs. The dimensionality of any material is determined by the number of spatial directions that electrons can move freely. In QDs, the free motion of the electrons is trapped in a quasi-zero dimensional "dot". Because of the strong confinement imposed in all three spatial directions, QDs behave similarly to atoms.

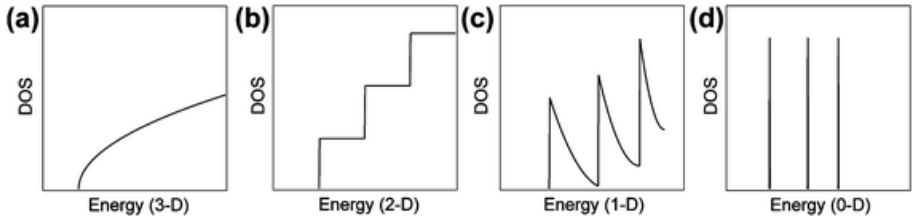

Figure 1.1: Density of states of a a) bulk material, b) quantum well, c) quantum wire and d) quantum dot.

When an electron is confined by a potential barrier, its continuous spectrum becomes discrete. In particular, the gap between two neighboring energy levels increases as the length where a free electron moves decreases. If the motion of electrons in the conduction band or that of the hole in the valence band is limited in a small region in the scale of De Broglie wavelength or Bohr exciton radius, the conduction band (CB) or the valence band (VB) is split into subbands or discrete levels depending on the dimensionality of the confined structure, therefore energy quantization or momentum quantization is observed and quantum effects become appearent. This phenomenon is known as the "size quantization effect".

Electronic characteristics of QDs are related to the size and shape of the individual crystal. As the size of NC gets smaller, the effective band gap and energy amount to be excited increases where the emission wavelength decreases.

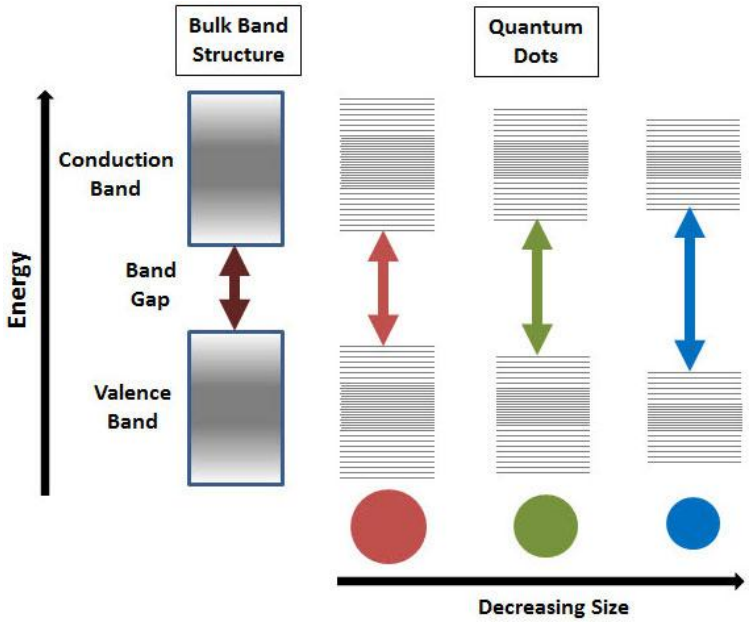

Figure 1.2: Band gap of QDs with different sizes in comparison to bulk form.

1.1.1.1 Basic quantum mechanics & energy band modelling

It is known that electrons moving in a solid are described by their total energy *E* and the wave function $\psi(\vec{r},\ t)$, which is a complex function of the position and time that carries all dynamic information regarding electrons' movement. $|\psi(\vec{r},\ t)|^2$ represents the probability per unit volume to find the electron around position "*r*" at the instant "*t*". This quantity is called as "probability density". Since the electron has to be somewhere, the probability density is normalized to a value of "1":

$$\int |\psi(\vec{r},\ t)|^2 \, d\vec{r} = 1 \qquad \textbf{(1.1)}$$

The energy of electron *E* and its wave functions are obtained by solving the time-independent Schrödinger equation:

$$\left[-\frac{\hbar^2}{2m}\nabla^2 + V(\vec{r})\right]\psi_n(\vec{r}) = E_n\psi_n(\vec{r}) \qquad \textbf{(1.2)}$$

The time-independent Schrödinger equation must be used only in problems where the time is not an important parameter. In the above equation, $\hbar$ = 1.05459 x 10^{-34} J.s is the reduced Planck constant, *m* is the electron mass and $V(\vec{r})$ is the position-dependent potential energy landscape acting on electron. For the electrons moving

freely in a medium (e.g in a vacuum), $V(\vec{r})$ equals to zero, thus results Schrödinger equation in:

$$-\frac{\hbar^2}{2m}\nabla^2\psi_n(\vec{r}) = E_n\psi_n(\vec{r}) \tag{1.3}$$

In contrast to the wave-like nature, electrons also have mass, which is a characteristic intrinsic to particles. The relationship between the particle-like and wave-like of electron is known as wave-particle duality and described by the De Broglie relationship:

$$\vec{p} = \hbar\vec{k} \tag{1.4}$$

Here, $k = 2\pi/\lambda$ is the wave vector, where λ is the electron wavelength. For an electron in a vacuum away from the influence of electromagnetic fields, the total energy E is just the kinetic energy T. Since $\vec{p} = m\vec{v}$, and the kinetic energy of a particle with momentum $\vec{p}$ and mass m, is given by $E = p^2/2m$, the electron energy in a vacuum is given by:

$$T = \frac{\hbar^2 k^2}{m} \tag{1.5}$$

The dispersion or energy versus momentum (which is proportional to the wave vector k) curves are parabolic just as for classical free particles.

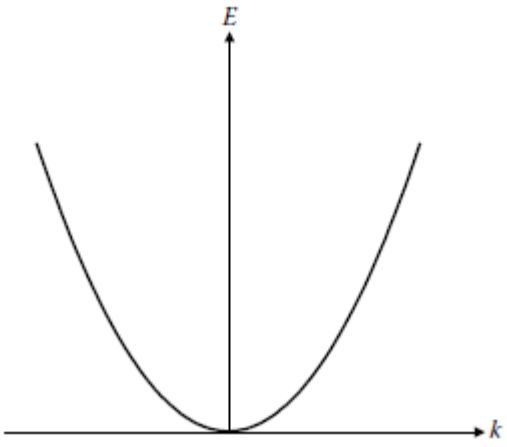

Figure 1.3: Energy dispersion relationship for a free particle.

Although equation (1.5) is the energy dispersion of electrons moving freely in vacuum, all solids have their own band structure. It turns out that, for small values of k, the band structure of bulk materials is nearly parabolic as in equation (1.5) with some modifications.

In real materials, there will be lattice defects within the structure at moderate temperatures, atoms vibrating around their lattice position and large number of electrons. Most of these electrons are bound to the host atoms and can not move around. Other electrons are released from the valence shell of the host atoms and are free to move through volume of the material due to temperature effects. When electrons are released from host atoms, they leave behind an available electron state (named as "hole") in the valence shell that can be filled by an electron either moving or bound to neighboring atoms. Holes behave like an electron with a positive charge. Moving electrons occupy electronic states in the CB, while the moving holes occupy electronic states in the VB. Thus, the band structure of real materials must be composed of conduction and valence band of energy.

The crystal structure of a bulk material is not a vacuum so that the average interactions of electrons and holes with host atoms and other electrons and holes are felt as if they have an effective mass m^*, which strongly differs from the electrons' rest mass in vacuum m_0, for most of materials.

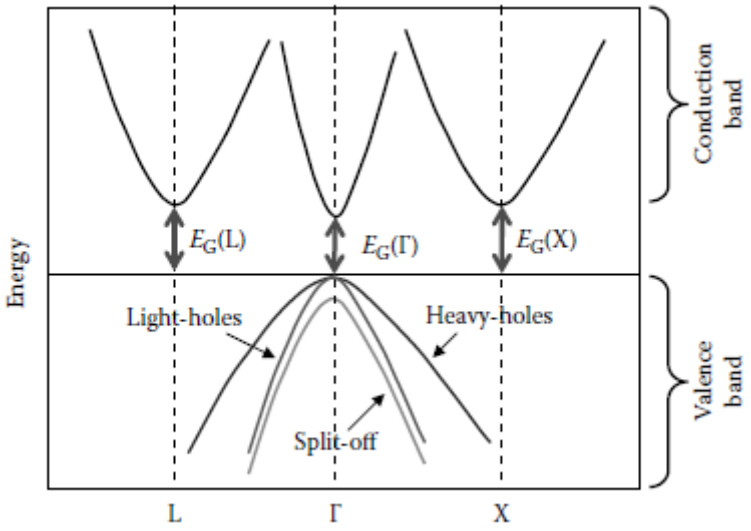

Figure 1.4: Energy versus momentum dispersion of bulk solids for small values of the momentum. Due to coupling effects of orbital motion around the host atom and electron spin, there are two types of holes, adapted from (Sattler, 2011).

In general, the curvature of the energy dispersion of electrons (see Figure 1.4) is different from the dispersion of holes. The minimum energy separation between the CB and VB is named as "energy band gap" (E_G). This energy indicates the amount of energy required to promote an electron from the VB to the CB. This quantity also gives a primary indication about the characteristic (metallic, semiconductor or insulator) of materials. Large E_G ($\geq$3 eV) indicates insulator materials, while small E_G (~0 eV or a few meV) indicates metallic materials. Intermediate values are the characteristic of semiconductor materials.

The other interesting characteristic of real materials is that the k values of minimum of the CB and of the maximum of the VB may not coincide. If they coincide, the material is known as "direct band gap material". Otherwise, it is known as "indirect band gap" material.

1.1.1.2 Core-shell QDs & heterojunctions

Chemically passivating the NC core with a thin shell of wide band gap semiconductor prevents chemical interaction with the inter-NC environment. Moreover, it allows substantional improvement of optical stability and exhibits greater tolerance to processing conditions necessary for incorporation into solid-state structures. Several wide band gap semiconductors have been epitaxially grown on the surface of colloidal NCs were reported [6, 12, 15-16]. It is even possible to grow two different shell layers on the NC surface [17-19]. The use of such radial heterostructures (core-shell QDs) enables the new options for further control of the QDs' electronic properties in terms of wave function engineering (electrons and holes).

Depending on the combination of materials used in the core and shell regions, it is possible to control the relation position of electrons and holes. When electrons and holes are spatially separated between core and shell, it is said that the QD exhibits type-II confinement (CdSe/CdTe QDs); otherwise, it exhibits type-I confinement (CdSe/ZnS and CdSe/CdS QDs).

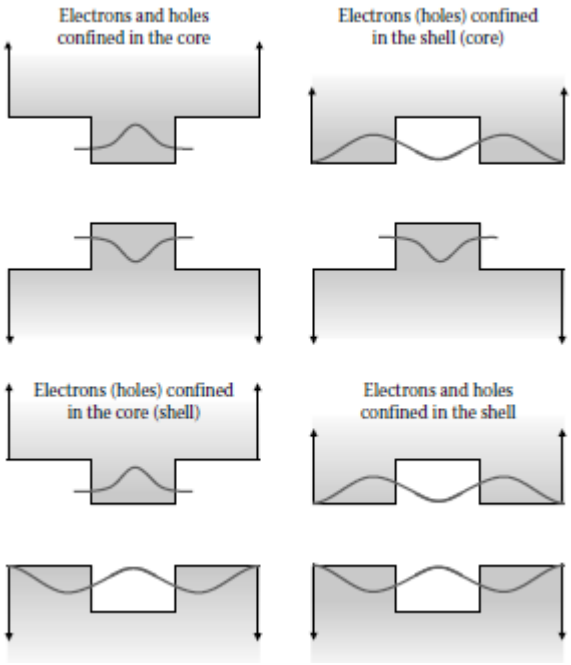

Figure 1.5: Possible band structure alignment in core-shell QDs, adapted from (Sattler, 2011).

Since core-shell QDs are composed of at least two different materials, each of them with their own band structures, it is necessary to understand how these band structures match at the interface [20]. Figure 1.6 shows the band structure of two different materials in contact. Assuming that two materials are identical, for an electron moves in the CB of the left material to the right, it crosses the interface without feeling it. If the materials are different as shown in the Figure 1.6, the electron sees an abrupt step between the bottom of the CB in the left and right. If the bottom of the CB in the right material is below the CB in the left, electrons gain energy in the right. On the other hand, if the CB in the right is above CB in the left, electrons see an energy barrier and are reflected at the interface. The same behavior is valid for holes.

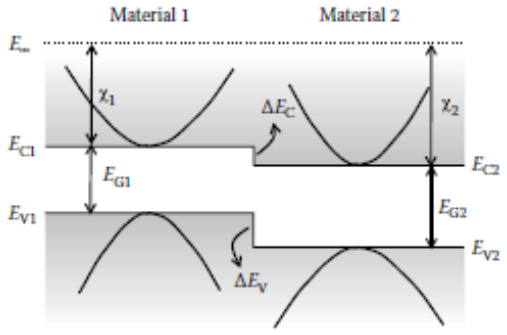

Figure 1.6: Band structure alignment near the interface of two different materials, adapted from (Sattler, 2011).

In core-shell QDs, the confinement potential is determined by the relative alignment of two materials. In this approximation, the alignments of band structures are made with respect to the energy necessary to remove an electron in the CB of the compounding materials. This energy amount is called as "electron affinity" and is denoted in χ . Thus, the energy barriers for electrons and holes between two different materials are obtained with:

$$\Delta E_C = |\chi_1 - \chi_2| \quad \textbf{(1.6)}$$

$$\Delta E_V = |(E_{G1} + \chi_1) - (E_{G2} + \chi_2)| \quad \textbf{(1.7)}$$

It is important to know that, this model is only valid when the lattice mismatch between the two materials is small. Otherwise, strain effects should be taken into account [21].

1.1.2 Optical properties of QDs

Semiconductor NCs have found large number of applications due to their changeable optical properties lie on different parameters such as crystalline size, composition rate and surface structure that discussed in previous chapters. Understanding the nature of these structures with all details before the production of potential applications is necessary for the control of luminescent properties (e.g. emission wavelength, quantum yield, luminescence lifetime and stability) during the synthesis and characterization steps.

Photoluminescence (PL) and optical absorption are the most usual experiments related with light emission used to investigate the optical properties of QDs. Photoluminescence is the optical radiation emitted by a physical system resulting from excitation to a nonequilibrium state by irradiation with light. If the incident photons have the energy of the same order with band gap of the material, the incident radiation creates electron-hole pairs, which remain free until they are captured at an imperfection or recombine directly with a hole releasing the energy absorbed. Recombination can occur spontaneously or stimulated by the incident light beam. If the released energy is delivered as photons, the recombination process is named radiative.

Once an electron-hole pair is created by the absorption of a photon, they interact with each other by means of their opposite charges, forming a quasi-particle called "exciton". The total energy of an exciton indicates the color (wavelength) of the light emitted by the quantum systems. The effect of band structure on optical absorption edge shifts due to quantum size effect is described theoretically by the effective mass approximation on the basis of two confinement regimes depending on whether the NC size (R_{NC}) to Bohr exciton diameter (R_B) ratios (R_{NC}/R_B) are ≤ 2 or ≥ 4 [22]. In the case of strong confinement in which electrons and holes are independently confined when the NC s are much smaller than R_B. The exciton energy on the size of NCs is given by;

$$E_X = E_{Bulk} + \frac{2h^2}{\mu}\left(\frac{\pi}{R_{NC}}\right)^2 \qquad \textbf{(1.8)}$$

where μ is the effective mass of electron-hole pair of masses m_e and m_h given by:

$$\frac{1}{\mu} = \frac{1}{m_e} + \frac{1}{m_h} \qquad \textbf{(1.9)}$$

In the weak confinement regime, when NC size is bigger than $4R_B$ exciton within the NCs, show translational motion confinement due to strong Coulomb interaction. The excitonic energy is given by the above relation except that the effective mass of electron-hole pair (μ) is replaced by the total mass of exciton $M = m_e + m_h$ and represented by:

$$E_X = E_{Bulk} + \frac{2h^2}{M}\left(\frac{\pi}{R_{NC}}\right)^2 \qquad \textbf{(1.10)}$$

Due to discrete energy levels of NCs, the photon absorption may occur via different mechanisms regarding the energy range of incident photons. In general, the electronic transitions caused by photons' absorption are divided into two types: Intraband and interband transitions. Intraband transitions occur exclusively between states within either CB or VB. In this case, the energy of incident photons is very low (a few meV), raging in the infrared region of the electromagnetic spectrum. Interband transitions involve transitions between VB and CB. The energy of photons for interband transitions is generally higher than for intraband transitions. Interband

transitions are only possible when the energy of incident photons is larger than the band gap energy of the material investigated.

Since the non-radiative transition is very fast, the energy structure of QDs can be simplified as a two-level system (Figure 1.7). The absorption and emission cross section can be related with McCumber relation [23];

$$\sigma_e(\nu) = \frac{g_1}{g_2}\sigma_a(\nu) exp\left[\frac{E_0 - h\nu}{kT}\right] \qquad \textbf{(1.11)}$$

where E_0 is the intrinsic energy gap between two transition levels which can be calculated from the first absorption peak, $\sigma_e(\nu)$ is the emission cross section, k is the Boltzmann constant and T is the temperature in Kelvin. g_i is the degeneracy of upper and lower levels.

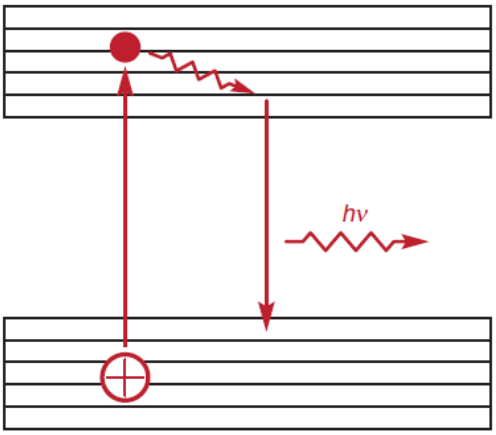

Figure 1.7: Absorption mechanism model for QDs.

2. SYNTHESIS

Since the NCs or QDs have tunable optical, electronic and chemical characteristics with respect to their size, shape and stoichiometry; there are numerous studies that focused on the synthesis of semiconductor QDs on a chemical route in order to obtain different properties such as narrow size distributions [24], surface modification to improve the luminescence efficiency [25] and colloidal stability of the particles [26]. Synthesis of monodisperse and small, well-controlled size QDs is difficult as most of methods are very sensitive to initial conditions and small variations at early stages of the nucleation process cause significant differences in NC size distributions.

CdSe NCs, a member of the II-VI semiconductor family with a direct band gap, are mostly investigated NCs due to their bright luminescence in the visible range of optical spectrum with varying particle size. CdSe QDs are produced in two different synthetic routes in general: Inorganic phase and aqueous phase approaches. QDs from the inorganic phase approach are insoluable in aqueous solution and therefore they are not compatible with a biological system. Water soluable CdSe QDs are generally synthesized in a water bath at temperatures below 100°C that requiring long time period (1-12 hours), where insoluable QDs are produced at relatively high temperatures via injection of inorganic precursors at a stage of synthesis.

Compared with other synthetic conditions, reaction temperature and time are kinetic parameters and can significantly influence the nucleation and growth of QDs. Since the monomer formation and nucleation steps as well as the subsequent growth into small nanoparticles may not be separated completely, a simple way to clarify the nucleation process of CdSe QDs is to end the synthesis with a reaction time as short as possible. This period changes with respect to operating temperature and choosen method for the synthesis of CdSe QDs. To obtain small particles and narrow size distribution, a low initial reaction temperature is preferred. Synthesis temperatures of

CdSe QDs vary between the room temperature [11] and higher temperatures about 300°C [27-28].

It is generally difficult to passivate both anionic and cathionic surface sites by organic ligands simultaneously. In particular, CdSe QDs were covered either with CdS [29-30] or with ZnS [25, 31] to establish a core-shell system where the band gap of the core lies energetically within the band gap of the shell material and the photogenerated electrons and holes are mainly confined inside the CdSe core.

There are different requirements to form an "ideal" core-shell NC both from a crystallographic and electronic point of view. First, to produce particles with high crystallinity, the core and shell materials should have similar parameters such that the shell growth happens in an epitaxial manner without the formation of defects. Second, the shell material should possess a much higher band gap than the core to suppress tunneling of charge carriers from the cores to the newly formed surface atoms of the shell.

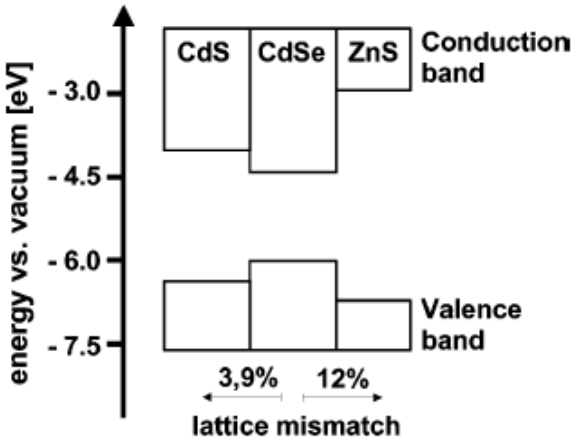

Figure 2.1: Energetic band positions and lattice mismatch of semiconductor CdSe/CdS and CdSe/ZnS combinations, adapted from (Xie *et al*., 2005).

Because of the ionic character within the shell materials CdS and ZnS is similar, the higher band gap in ZnS can be attributed to smaller interatomic distance with respect to CdS. The band offsets for the most commonly used core-shell CdSe/ZnS NCs are as high as 0.6 eV for the valence band and 1.44 eV for the conduction band, which leads to an appreciable electronic passivation. However, the lattice mismatch between CdSe and ZnS is in the order of 12%. Because of the large mismatch, the interface strain accumulates with increasing shell thickness and eventually can be

released through the formation of misfit dislocations, degrading the optical properties of NCs. Lattice defects can act as trapping sites for the photogenerated charge carriers and cause the formation of particles with irregular shape and broad size distribution upon increasing ZnS shell thickness.

For the material combination of CdSe cores with CdS shells, the interatomic distance is more similar and the lattice mismatch is only 3.9%, which favors the epitaxial growth. On the other hand, the lower band offsets with respect to ZnS (Figure 2.1) hamper the electronic passivation due to extended wave functions across the shell. To combine the advantages of both shell materials, multi-shell coverage methods are used in order to reduce lattice parameter difference [16-18].

2.1 Experimental Study

2.1.1 Synthesis of CdSe core QDs

For the synthesis of CdSe core NCs, the method developed by Zhu *et al*. [31] has been modified to use with facilities we have in our NANOSEMLAB - Nanostructure Semiconductor Research Labrotary. Firstly, cadmium stearate ($C_{36}H_{70}CdO_4$), the Cd precursor, is prepared by heating the mixture of CdO (0.01 mol, 1.284 g) and stearic acid ($C_{18}H_{36}O_2$) (0.02 mol, 5,68 g) at 170°C for 15 mins in order to use in further reactions. For a typical synthesis of CdSe core NCs, cadmium stearate (0.1358 g, 0.2 mmol) is added into a three-neck flask with 16 mL paraffin liquid without Se precursor as the Se can't be dissolved without any phosphine-based material at relatively lower temperatures than used in original method. To overcome this situation, 2 mL TOP and Se powder (0.0078 g, 0.1 mmol) are added into a flask and are mixed in an ultrasonic cleaner at the room temperature for several seconds. The cadmium stearate-paraffin mixture is degassed in vacuum at room temperature and then is heated to a desired temperature (160-180°C) with oil-bath heating for reaction under N_2 flow. When the heat is arised to aimed temperature, TOP-Se solution is rapidly injected into the reaction flask for the nucleation and growth of CdSe NCs.

Aliquots are taken at different time intervals via a syringe to monitor the growth of CdSe core NCs. After cooling down to room temperature, aliquots are centrifuged by addition of acetone at least three times to purify core solution. The end products are heated up to 60°C under vacuum to get rid of remaining solvents.

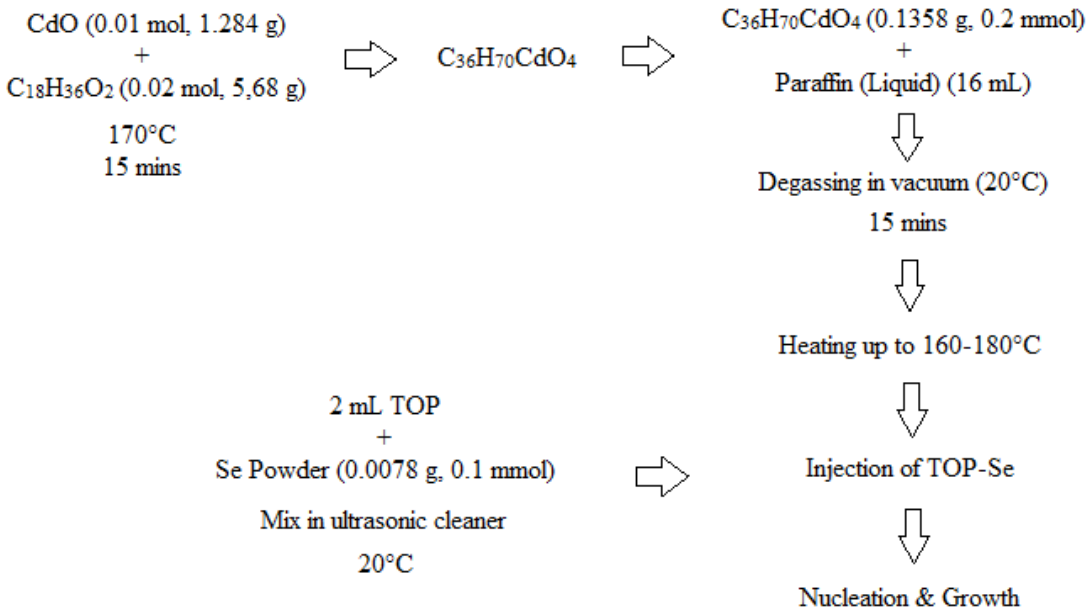

Figure 2.2: Typical synthesis procedure for CdSe core QDs.

To investigate the effect of temperature, time and initial ratio of the precursors on nucleation and growth kinetics; different combinations can be tried for synthesis of CdSe core QDs. Size quantization effect can be seen on Figure 2.3 clearly. Color transition from light yellow to red indicates the growth of NCs, thus resulting as decrease in the optical absorption band gap.

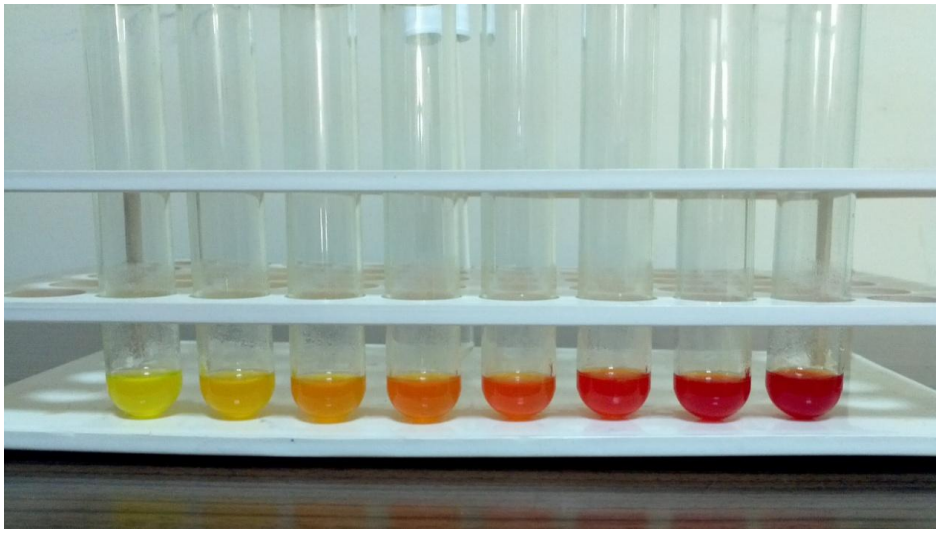

Figure 2.3: CdSe core QDs synthesized at 160°C with Cd:Se ratio of 1:10.

2.1.2 Growth of ZnS shells on CdSe core QDs

After collecting total 8 mL of samples by the end of CdSe core synthesis; the resulting core solution, $Zn(OAc)_2.2H_2O$ (0.085 mmol, 0.01866 g) and S powder (0.085 mmol, 0.00272 g) are mixed together in the reaction flask. The reaction

volume is adjusted to 15 mL by adding paraffin liquid. Then the mixture is degaseed at 80°C for 20 mins. Afterward, reaction temperature is set to 145°C for the shell growth under N_2 atmosphere. Aliquots are taken at different time intervals to monitor the shell growth. To grow ZnS shells with different thicknesses around the CdSe core, a seeding-growth technique [32] was adapted. By the end of each cycle, the same amount of Zn and S precursors are added into reaction flask and volume is adjusted to initial value by adding lack of paraffin liquid to complete 3 cycles until a desired core-shell NCs are obtained. The final products are precipitated by addition of acetone with a centrifuge step. After the centrifuging, aliquots are dried at 60°C under vacuum to get rid of remaining solvents for further processing.

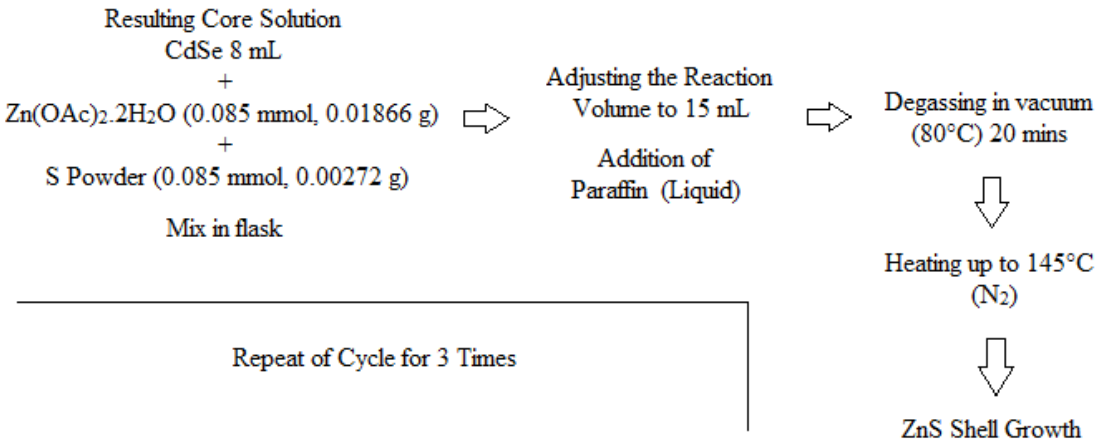

Figure 2.4: Typical synthesis procedure for ZnS shell growth on CdSe core NCs.

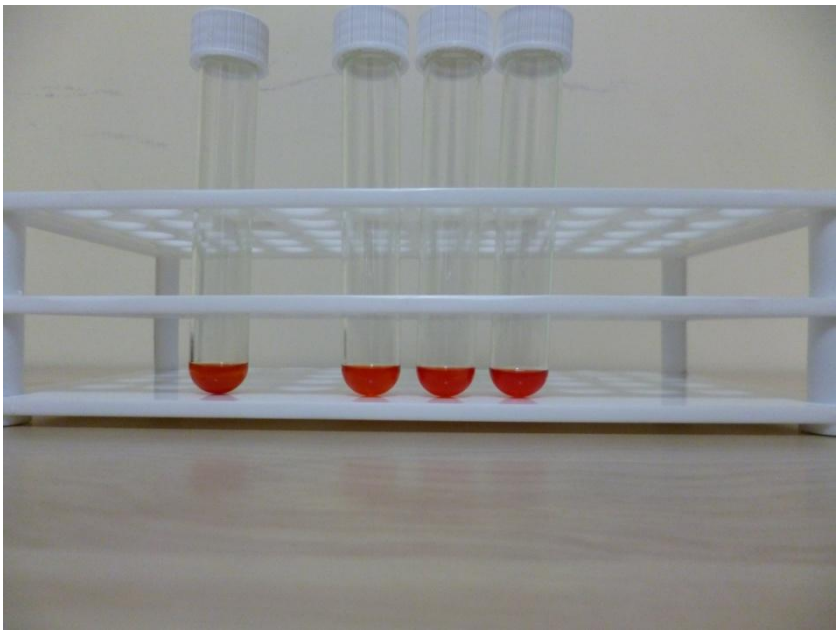

Figure 2.5: CdSe core QDs (left) synthesized at 160°C with a Cd:Se ratio of 1:1.25 and CdSe/ZnS core-shell QDs (right) covered over at 145°C within 3 cycles.

During the synthesis of both CdSe core NCs and CdSe/ZnS core-shell structures, a well-ventilated fume is used to avoid release of hazardous gases or molecules into the ambient due to TOP usage. Layout of synthesis can be seen in Figure 2.6.

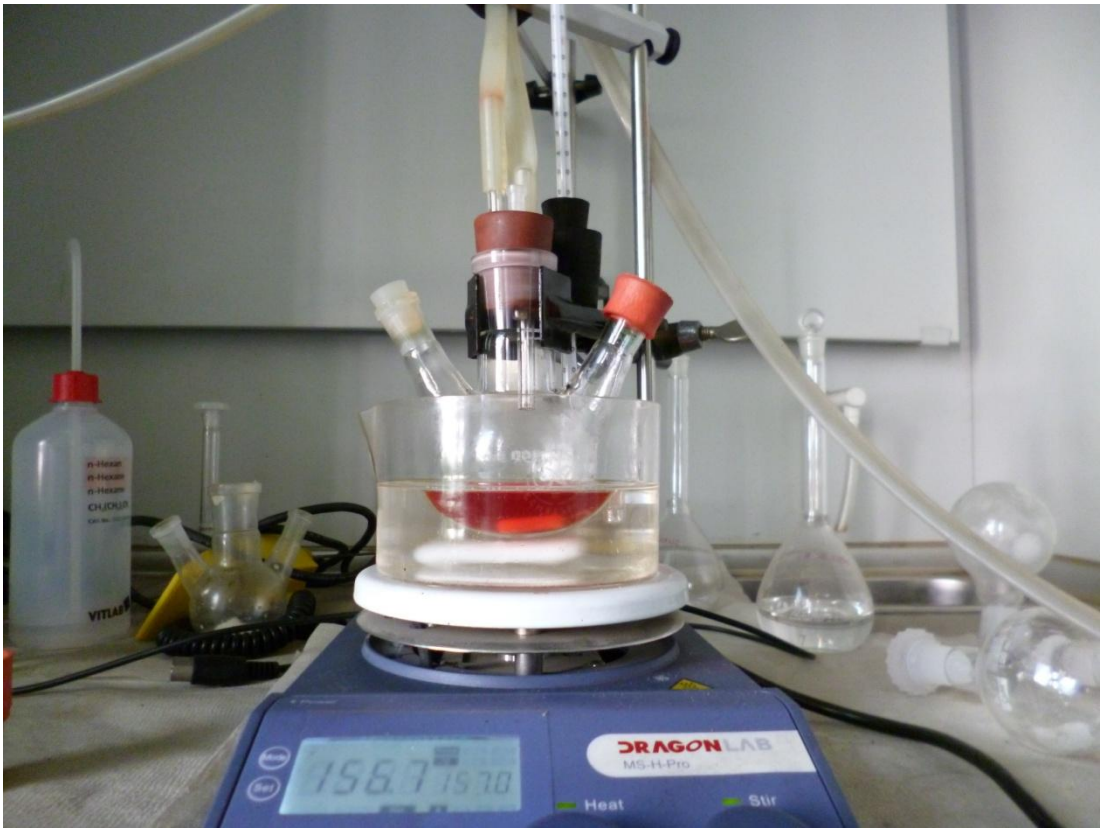

Figure 2.6: Layout of equipment for synthesis of CdSe and CdSe/ZnS NCs.

3. CHARACTERIZATION

3.1 Optical Characterization of CdSe & CdSe/ZnS QDs

It is known that UV-VIS absorption spectroscopy is one of the common analytical tool used in the characterization of CdSe QDs as the lowest energy absorption feature (the first exciton) can yield information on the band gap, particle size and size distribution [33]. The size-dependent optical properties of CdSe QDs were investigated by changing the temperature and initial precursor ratio throughout the experimental studies. The absorption spectra of CdSe QDs were obtained from Shimadzu UV-3600 UV-VIS-NIR Spectrophotometer. Increasing absorption peak values (wavelength in nm) with temperature and elapsed time, named as red shift, state the growth of NCs and quantization effect which is an expected behavior and well-matched with common studies [11, 15-16, 25, 31].

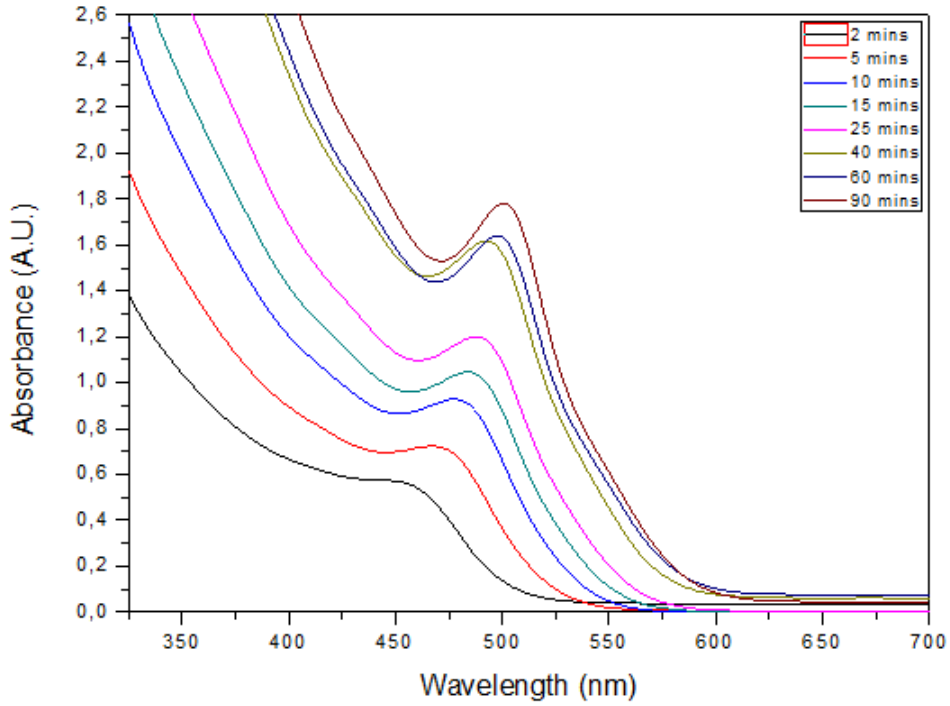

Figure 3.1: Absorption spectra of the CdSe QDs synthesized at 160°C with Cd:Se ratio of 1:5.

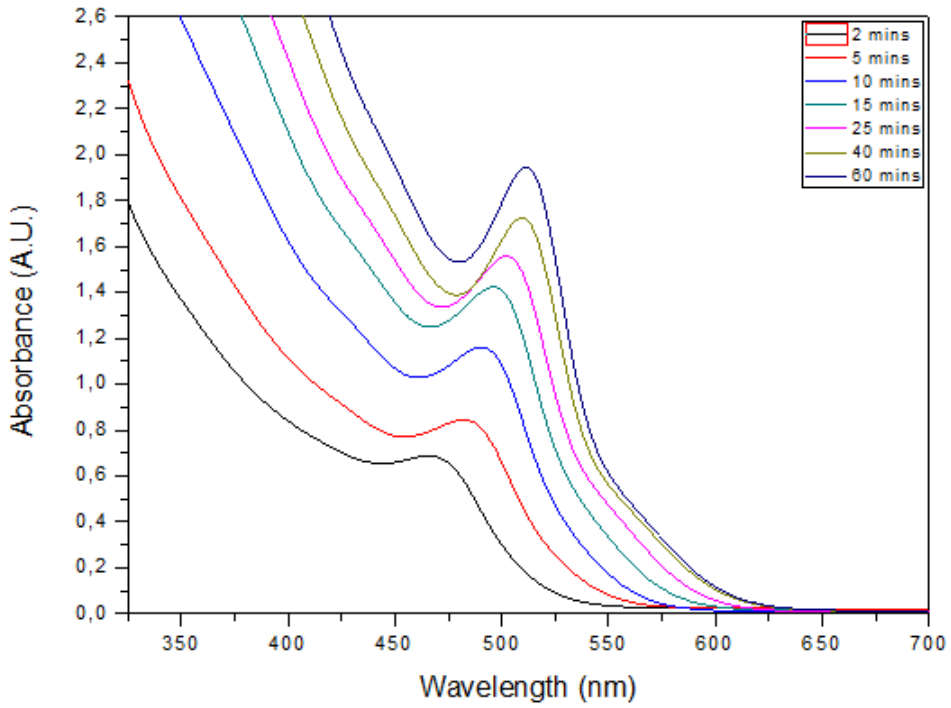

Figure 3.2: Absorption spectra of the CdSe QDs synthesized at 170°C with Cd:Se ratio of 1:2.5.

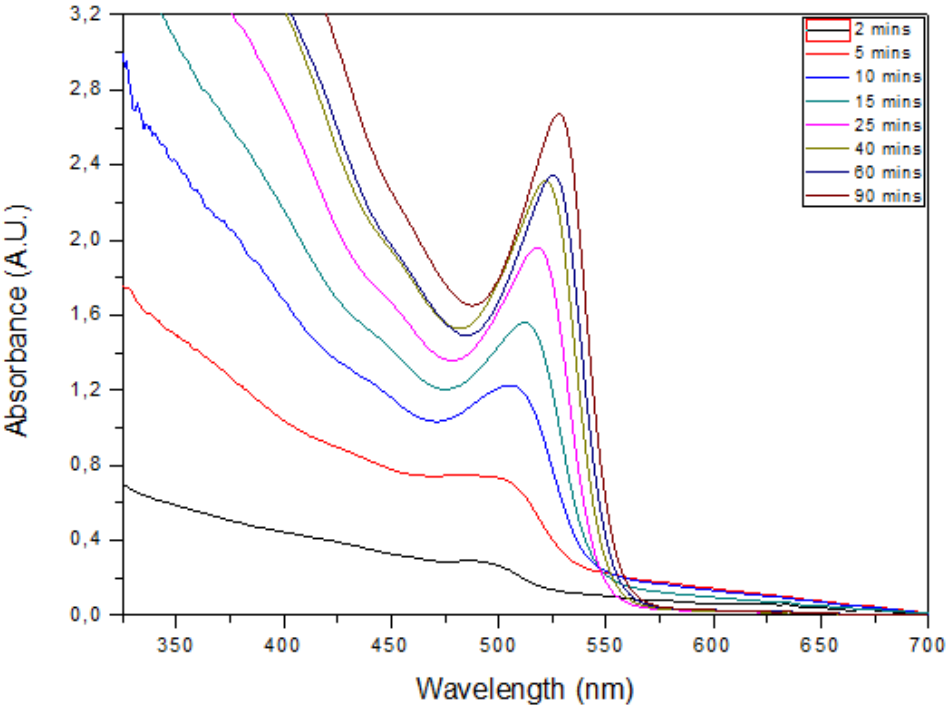

Figure 3.3: Absorption spectra of the CdSe QDs synthesized at 160°C with Cd:Se ratio of 1:1.25.

The absorption spectras were obtained from solutions that CdSe QDs are diluted in *n*-hexane. For each synthesis, the amount of hexane addition was kept as certain times the amount of CdSe QDs precisely.

Although there is no clear color transition in Figure 2.5, the red shift in the absorption spectra indicates the growth of ZnS shells over CdSe core QDs (Figure 3.4). The wavelength of absorption peak gets longer as the thickness of ZnS shells increase.

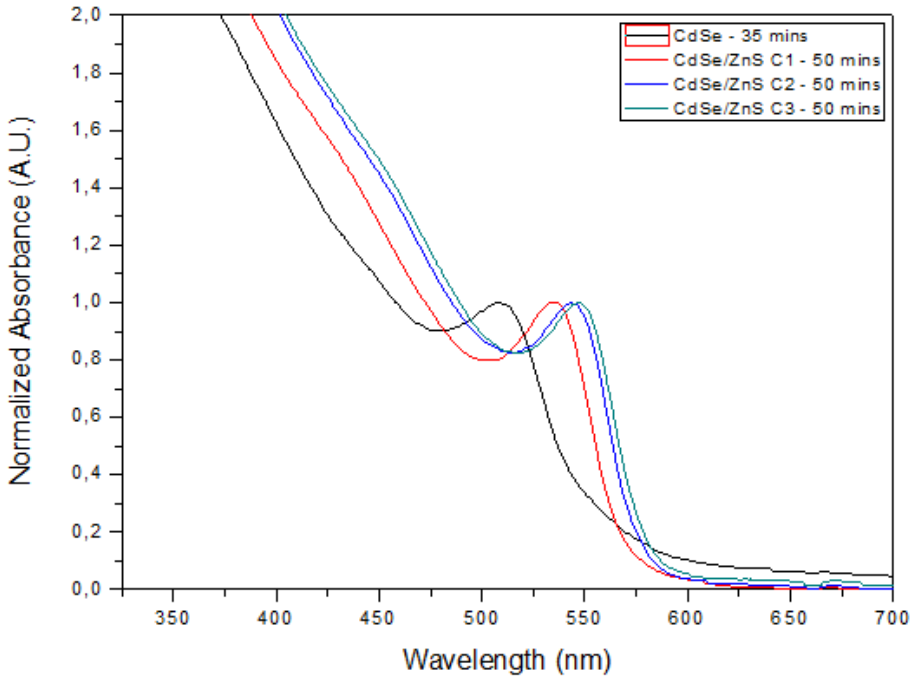

Figure 3.4: Normalized absorption spectra of CdSe QD – 35mins sample synthesized at 160°C with Cd:Se ratio of 1:1.25 and CdSe/ZnS core-shell QDs grown on throughout the number of cycles.

The variation of absorption coefficient (α) with photon energy ($h\nu$) at the band edge is not very sharp thus indicating band-tailing effect for these NCs. With modifying Mc Cumber relation **(1.11)** to CdSe QDs, the absorption coefficient can be expressed by;

$$\alpha = \alpha_0 exp\left[\frac{(h\nu - E_0)}{\varepsilon}\right] \qquad \textbf{(3.1)}$$

where E_0 and α_0 are the characteristic parameters of given material. $\varepsilon = kT/\sigma$ and degeneracy of upper and lower levels in Mc Cumber relation (g_1 and g_2) are equal to each other for CdSe. Using the random phase approximation for semiconductors, the following equation is obtained by assuming the CB and VB are nearly parabolic;

$$\alpha h\nu = A\left(h\nu - E_g\right)^n \qquad \textbf{(3.2)}$$

where n is a parameter related with density of states and equal to "$1/2$" for direct transitions or "2" for indirect transitions. Extrapolating the straight part of the plot of $(\alpha h\nu)^2$ versus $h\nu$ allows us to determine the optical absorption band gap of NCs.

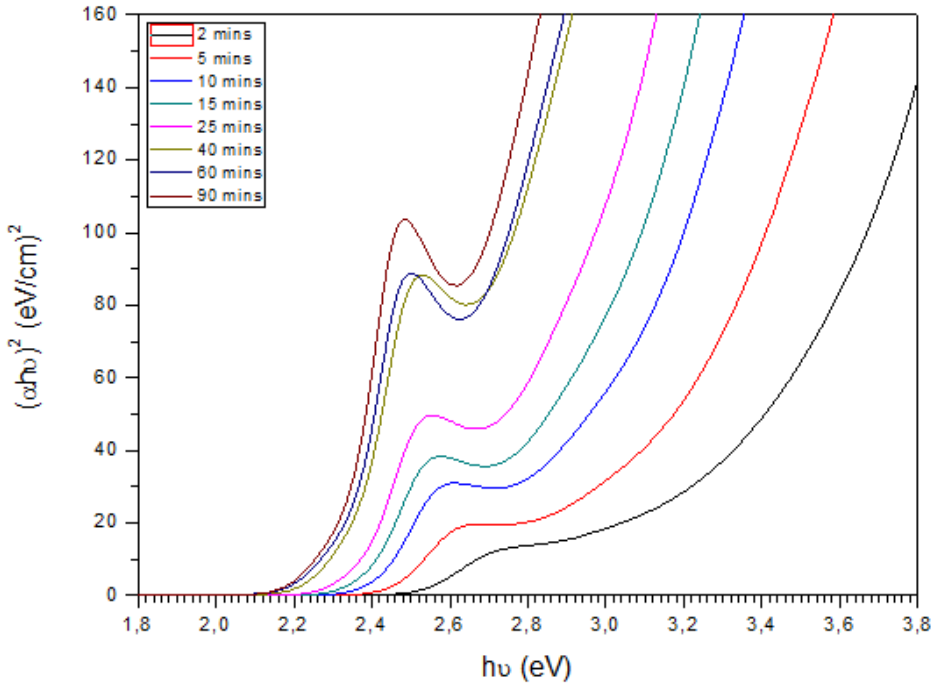

Figure 3.5: $(\alpha h\nu)^2$ vs. $h\nu$ plot of CdSe QDs synthesized at 160°C with Cd:Se ratio of 1:5.

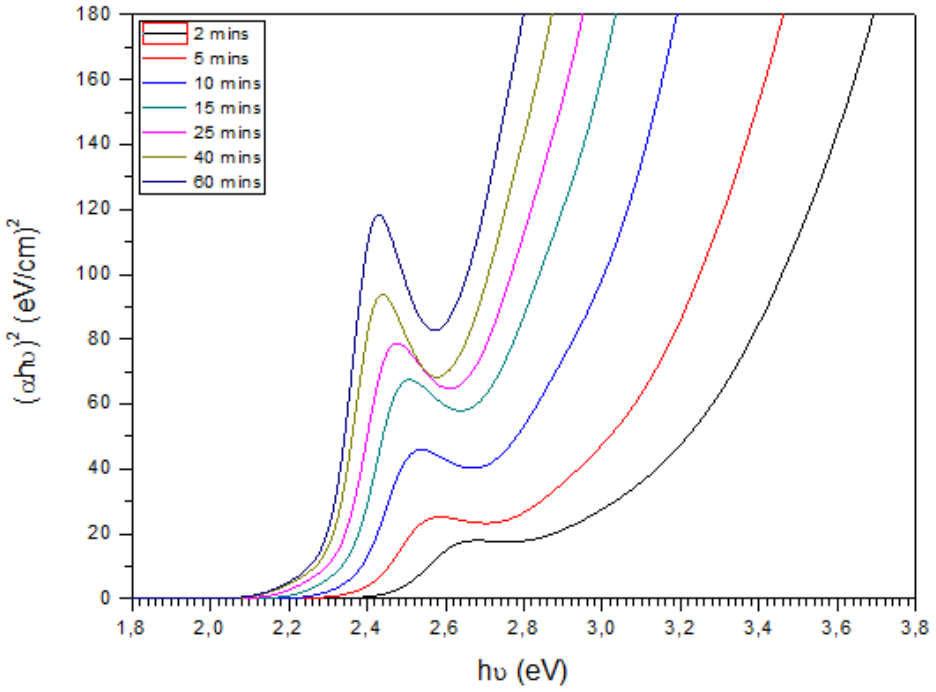

Figure 3.6: $(\alpha h\nu)^2$ vs. $h\nu$ plot of CdSe QDs synthesized at 170°C with Cd:Se ratio of 1:2.5.

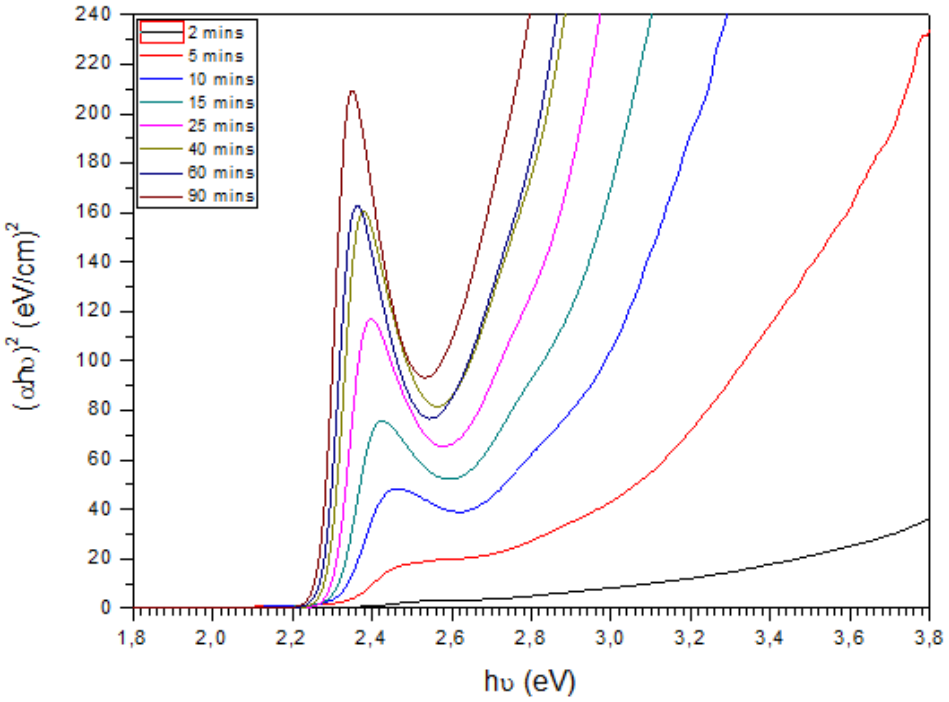

Figure 3.7: $(\alpha h\nu)^2$ vs. $h\nu$ plot of CdSe QDs synthesized at 160°C with Cd:Se ratio of 1:1.25.

3.2 Photoluminescence of CdSe & CdSe/ZnS QDs

Colloidal semiconductor QDs made from II-VI and III-V groups of the periodic table are found such a new class of fluorescent labels that is frequently employed in fluorescence imaging [34-35]. PL brightness, measured by PL quantum yield (QY) and the stability of the emission of QDs strongly depend on synthesis route. Generation of the inorganic outer layer (shell) is the most critical step for producing highly emissive materials. This layer ensures that the materials possess the exceedingly high and stable QYs (>30%) which are pivotal for imaging and light emitting/absorbing applications. Importance of the shell layers was first identified by Hines *et al*. after coating CdSe NCs with ZnS [36]. Since that effort, all types of QDs have been prepared with appropriate shells and core-shell systems are now default structures for QDs.

Qu and Peng (2002), have been investigated the influence of the initial ratio between Cd and Se precursors on the temporal evolution of the ensemble PL QY of CdSe NCs during their growth in a coordinating solvent. The PL QY was observed to increase monotonically during growth to a maximum value (named as bright point) and then gradually decrease. The position and temporal width of the bright point, the

highest QY, the growth kinetics and the sharpness of the PL peak were all reported to be strongly dependent on the initial Cd:Se ratio. The existence of the bright point was interpreted as a signature of an optimal surface structure of the NCs grown under given conditions [37].

Talapin *et al*. (2002) investigated the distribution of properties within ensembles of collodially grown CdSe NCs by analyzing size-selected fractions. An excess of the metal cation precursor (Cd) was used and a huge difference was observed between the PL efficiencies of fractions size-selected from the same ensemble. This behavior was attributed to differences in surface disorder of the NCs as a consequence of the Ostwald ripening growth mechanism. The particles with the lowest growth rate within the ensemble were assumed to have the lowest degree of surface disorder and therefore the highest PL QY at any given reaction conditions [38].

Donegá *et al*. (2003) have found out the critical operation temperature as 240°C for obtaining high PL QYs from CdSe NCs with given synthesis route. Below this equilibrium point, an increase in the temperature improves the PL QY, even though the ensemble rates become larger. The lower PL QYs they achieved below 240°C imply that there is activation energy for surface ordering and reconstruction where the higher temperatures induce faster surface degradatiton that reduces the luminescence efficiency shortly after the maximum efficiency has been reached. They also figured out that surface degradation can be stopped by quenching the ensemble of CdSe NCs with the optimum surface to room temperature [27].

Although there are numerous studies that cover the determination of PL QY for each individual synthesis route, most of them have not clearly addressed the detailed calculation of luminescence efficiency. Grabolle *et al*. (2009), have successfully demonstrated the determination of PL QY of QDs in different methods with using various reference dyes. They also have showed how to control luminescence properties with instruments and tuning absorption wavelengths of specimens [39].

FWHM value is another good way to understand the quality of synthesized NCs where smaller values indicate the monodispersity of grown species. Typical FWHM values of the PL peak of the CdSe NCs vary between 25-40 nm at room temperature.

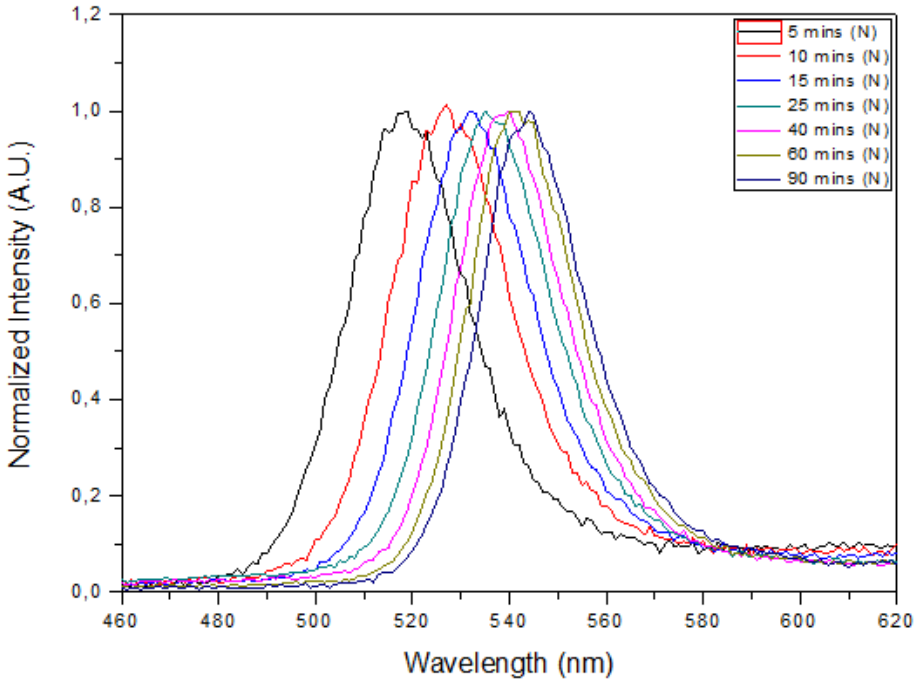

Figure 3.8: Normalized PL spectra of CdSe QDs synthesized at 160°C with Cd:Se ratio of 1:1.25.

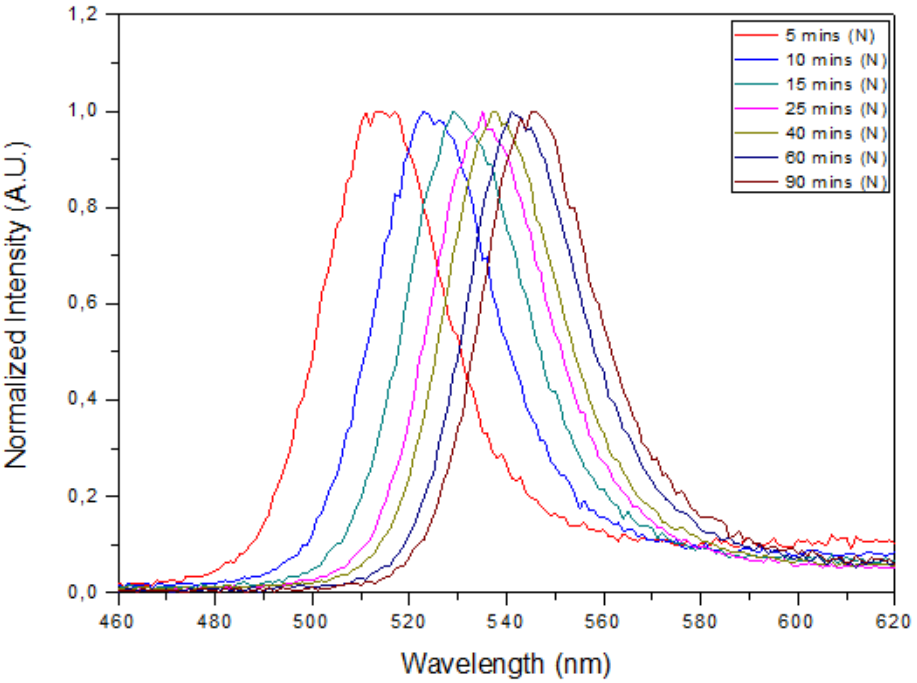

Figure 3.9: Normalized PL spectra of CdSe QDs synthesized at 170°C with Cd:Se ratio of 1:1.25.

Analysis of PL features was done via Varian Cary Eclipse Fluorescence Spectrophotometer. The aliquots were diluted with *n*-hexane directly for characterization. The PL QY of NCs were estimated in comparison with Rhodamine

6G in methanol, assuming its PL QY as 95% (at 528 nm) and using data derived from the luminescence and absorption spectra by using the following procedure:

$$\Phi = \Phi_S \left(\frac{I}{I_S} \right) \left(\frac{A_S}{A} \right) \left(\frac{n^2}{n_S^2} \right) \quad \textbf{(3.3)}$$

In the equation above, I (sample) and I_s (standard) are the integrated emission peak areas upon choosen excitation wavelength, A (sample) and A_s (standard) are the absorption at excitation wavelength, n (sample) and n_s (standard) are the refractive indices of the solvents, Φ and Φ_S are the PL QYs for the sample and the standard.

3.3 Morphological Analysis & Determination of NC Diameter

The diameter of semiconductor NCs were estimated by using datas converted from absorption peak values to photon excitation energy values in the below equation obtained as a result of effective-mass approximation:

$$E_{1s,1s}(d) = E_g + \frac{2\hbar^2\pi^2}{d^2}\left[\frac{1}{m_e^*} + \frac{1}{m_h^*}\right] - \frac{3.572e^2}{\varepsilon d} - \frac{0.124e^4}{\hbar^2\varepsilon^2}\left[\frac{m_e^* m_h^*}{m_e^* + m_h^*}\right] \quad \textbf{(3.4)}$$

In the equation above, $E_{1s,1s}(d)$ is the peak value of first electron-hole pair, E_g is the band gap of bulk material (1.74 eV for CdSe), $m_e^* = 0.13\, m_0$ and $m_h^* = 0.43\ m_0$ are the effective masses of electron and holes in CdSe and $\varepsilon = 5.8\,\varepsilon_0$ is the optical dielectric constant of CdSe where d is the diameter of semiconductor NC. The second term gives the kinetic energy of electron-hole pair, third term belongs to Coulomb interaction and the last term determines the correlation energy between two particles.

To verify the correction of calculated NC diameter values of different synthesis routes, HRTEM analysis was performed by using FEI Tecnai G2 F30 in National Nanotechnology Research Center (UNAM) located at Bilkent University. The average diameter values obtained from HRTEM images are well-matched with theoretically calculated values. Due to existence of paraffin liquid despite the number of centrifugation processes, the images of higher magnifications are blurred to observe crystallinity of NCs clearly. However, narrow size distribution can be easily identified.

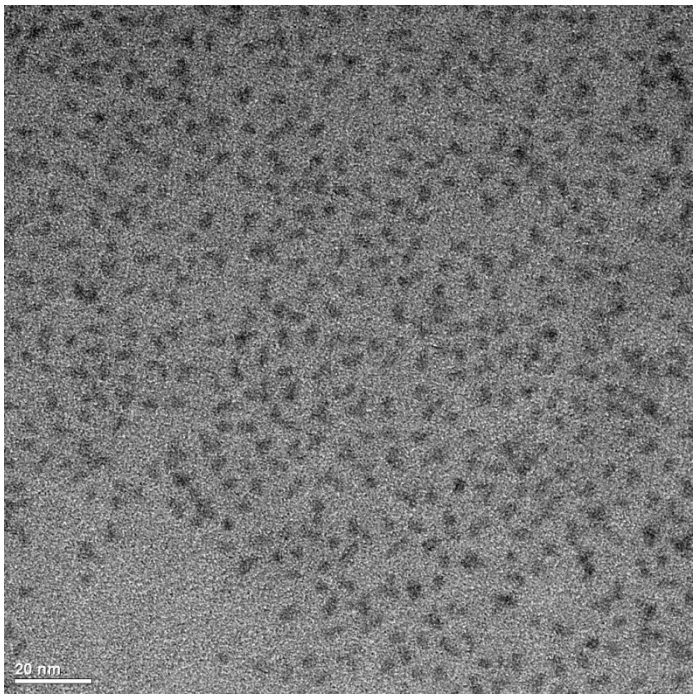

Figure 3.10: HRTEM image of CdSe QDs synthesized at 170°C with Cd:Se ratio of 1:5. The label is indicator of 20 nm length. The average diameter is 3±0.3 nm where the calculated value is 2.984 nm.

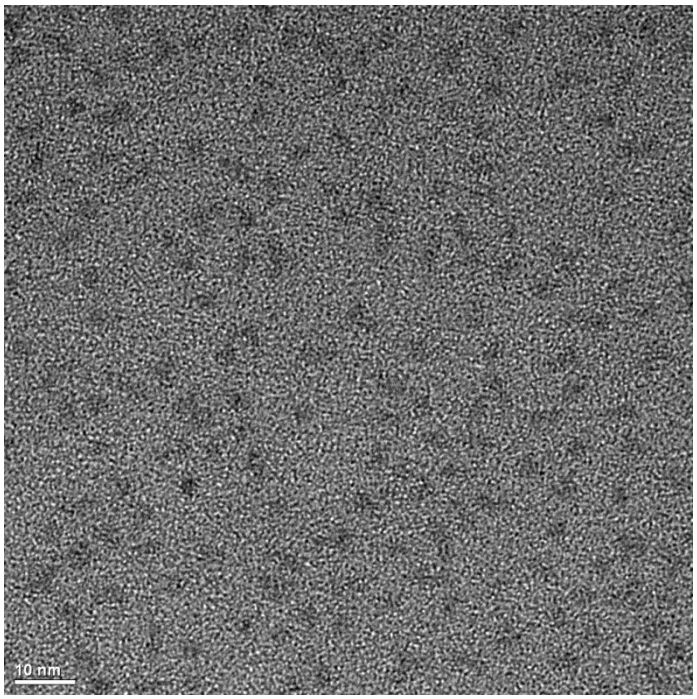

Figure 3.11: HRTEM image of CdSe QDs synthesized at 170°C with Cd:Se ratio of 1:5. The label is indicator of 10 nm length. The average diameter is 3.1±0.2 nm where the calculated value is 2.984 nm.

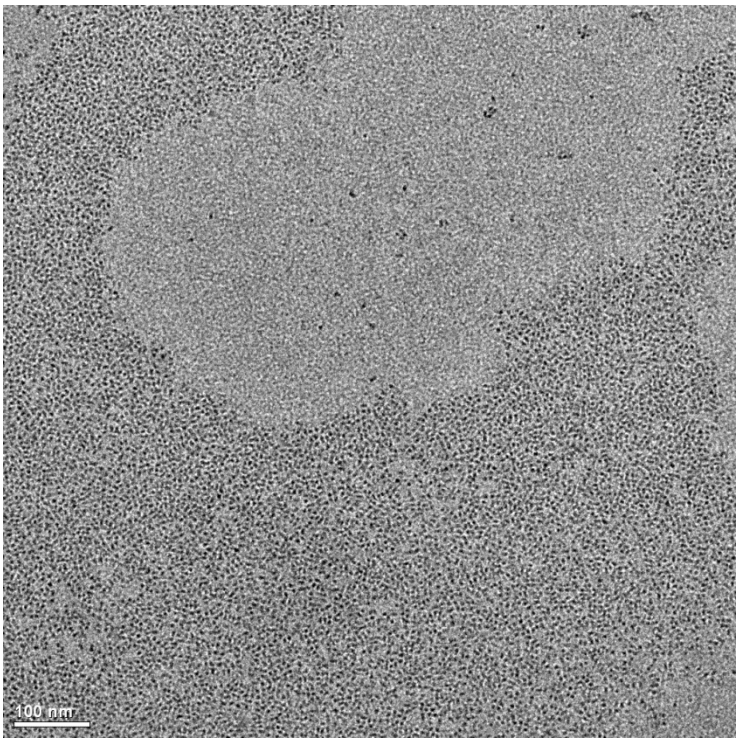

Figure 3.12: HRTEM image of CdSe QDs synthesized at 160°C with Cd:Se ratio of 1:2.5. The label is indicator of 100 nm.

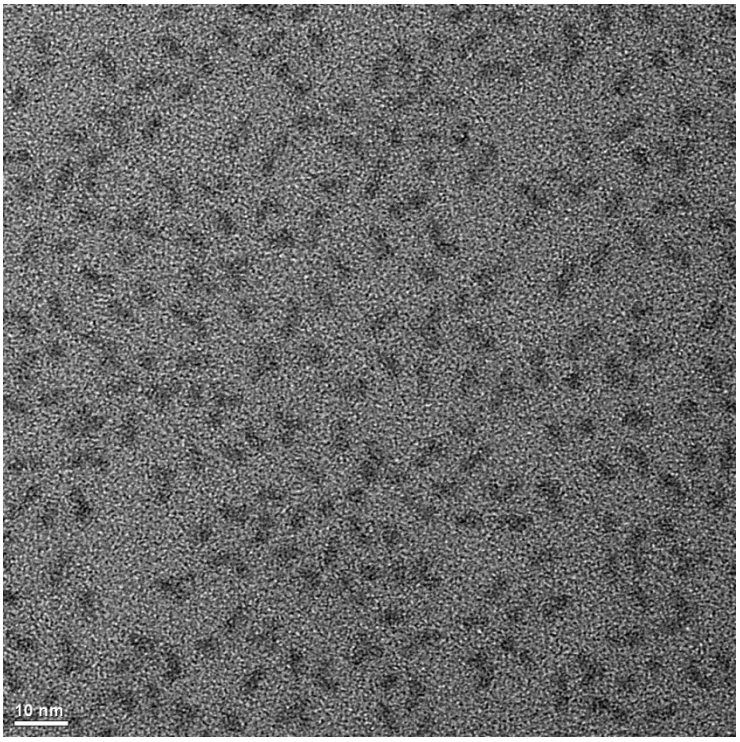

Figure 3.13: HRTEM image of CdSe QDs synthesized at 160°C with Cd:Se ratio of 1:2.5. The label is indicator of 10 nm. The average diameter is 3.1±0.2 nm where the calculated value is 2.944 nm.

XRD pattern of CdSe/ZnS core-shell nanocrystals that obtained from Rigaku SmartLab X-Ray Diffractometer placed at ITUNANO – Nanotechnology Research Center with a Cd:Se initial precursor ratio of 2:1 where the core CdSe nanocrystals were synthesized at 170°C is shown in the Figure 3.14. Two diffraction peaks corresponding to the (111) and (311) lattice planes of ZnS shells match bulk cubic (zinc blende) peaks where the (220) lattice plane of CdSe cores match bulk cubic (zinc blende) peaks, as found in originated article [31].

Diffraction peaks are broad because of the finite size of nanocrystals. Diffraction angle values indicate the formation of ZnS shells over CdSe core nanocrystals as peak positions of ZnS shells shift to higher scattering angle than CdSe bulk values when it compared to literature database.

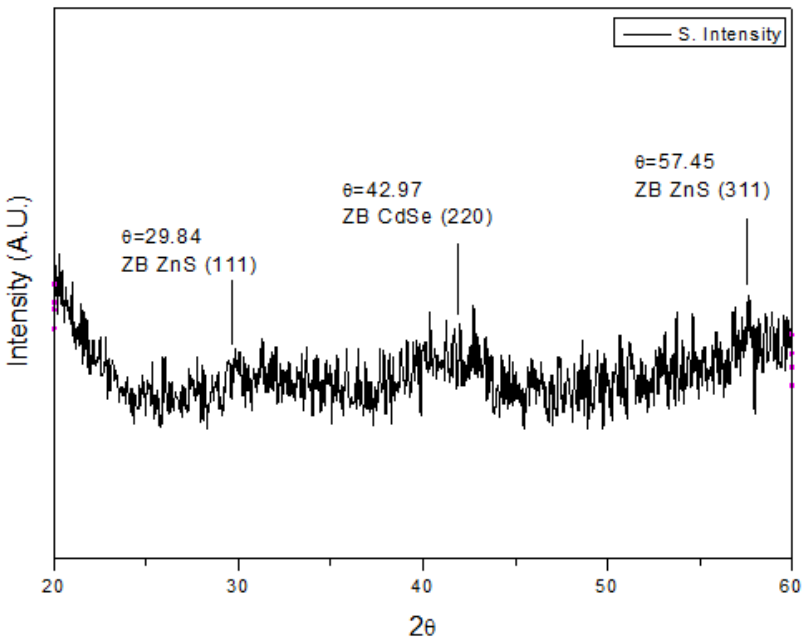

Figure 3.14: XRD pattern of the CdSe/ZnS core-shell QDs with Cd:Se precursor ratio of 2:1 (CdSe synthesis temperature: 170°C). Lattice planes correspond to JCPDS file No. 77-2100 for ZnS shell and JCPDS file No. 19-0191 for. CdSe core.

4. RESULTS & DISCUSSION

4.1 Effect of Temperature & Precursor Ratio on the NC Growth

Since the growth kinetics of semiconductor NCs are dependent on temperature, time and initial precursor ratio for any synthesis route, influence of changes in these variables on the final properties CdSe QDs were investigated. The most important parameter, Cd:Se molar ratio of the precursors; was found having the ability of change the average particle size, number of density and size distribution by "focusing" and "defocusing" the particle growth in the solution [10].

Figure 4.1 shows the diameter distribution of NCs grown with different Cd:Se molar ratios at given synthesis temperature. As the amount of Cd precursor increases, NCs grow into larger diameters very fast and growth is the predominant process over nucleation, which reduces the number of density and increases the average particle size under same experimental conditions, coherent with the study of Bhattacharjee *et al*. [40]. Increase in the NC diameter is also responsible for red shift in the emission and absorption spectra of CdSe QDs.

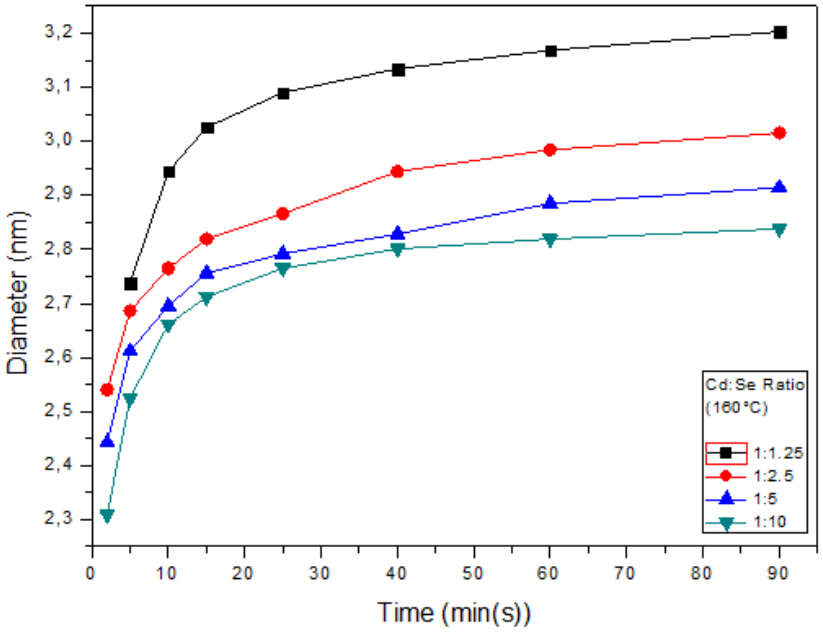

Figure 4.1: Growth of CdSe NCs with different Cd:Se molar ratios at 160°C.

On the other hand, the operating temperature influnces the growth of NCs when it compared in identical chemical compounds and elapsed time. As shown in the Figure 4.2-4.4, difference in the diameter of grown NCs increases with the excessive amount of initial Se precursor, therefore indicating that the effect of operating temperature is evident for the Se rich samples. However, lower temperatures are not suitable for the ideal growth of Cd rich samples.

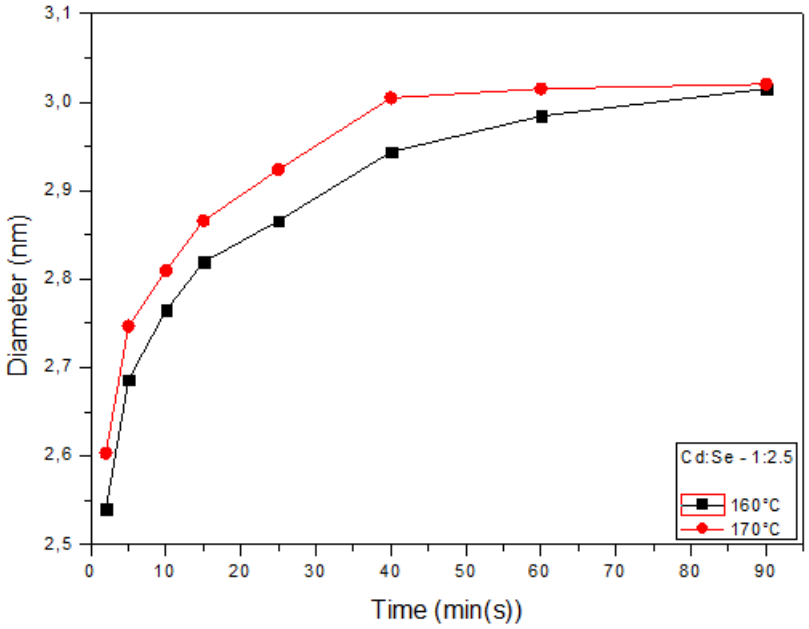

Figure 4.2: Effect of temperature on CdSe NCs growth for Cd:Se ratio of 1:2.5.

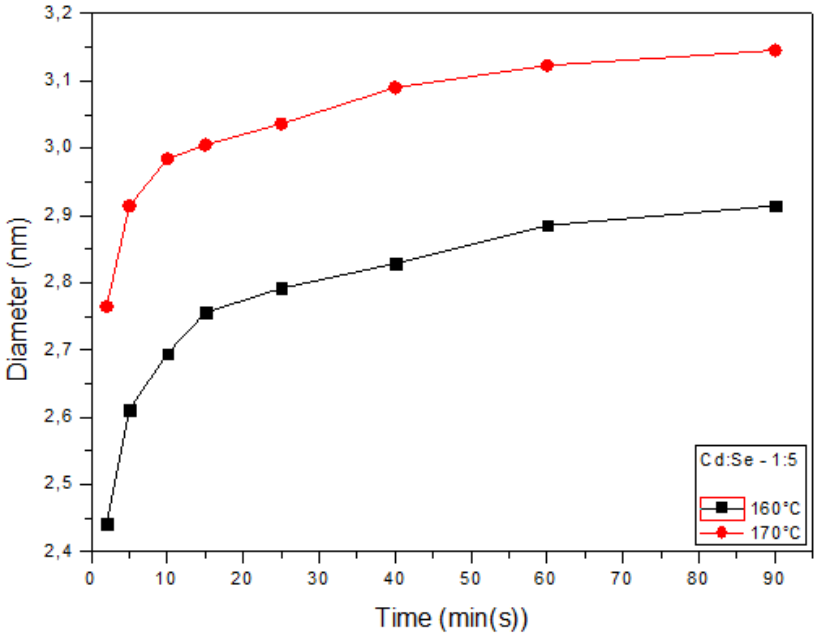

Figure 4.3: Effect of temperature on CdSe NCs growth for Cd:Se ratio of 1:5.

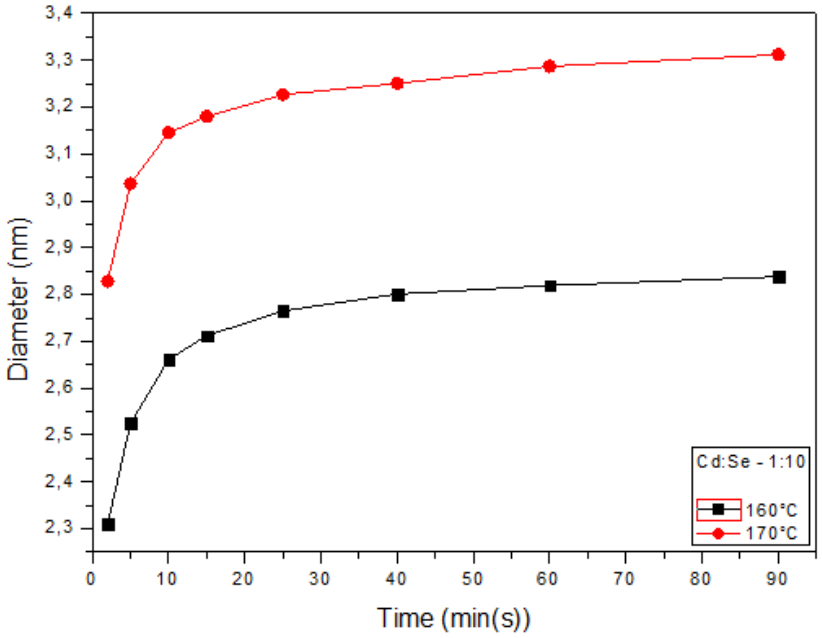

Figure 4.4: Effect of temperature on CdSe NCs growth for Cd:Se ratio of 1:10.

4.2 Emission Quality & Photoluminescence Quantum Yield of NCs

FWHM of an emission peak is the measure of color purity of the emission where the smaller values indicate more pure emission and narrow size distributions without Ostwald ripening (Figure 3.8-3.9). Table 4.1 shows the average FWHM values obtained from PL spectras with respect to various conditions. It is noticable that, the average FWHM value increase as the initial Cd:Se precursor ratio decreases.

Table 4.1: Effect of Cd:Se initial precursor ratio on the average FWHM values of CdSe NCs.

Sample	Molar Ratio	Temperature	Average FWHM
CdSe	1:1.25	170°C	29.856 nm
CdSe	1:5	170°C	30.156 nm
CdSe	1:10	170°C	30.956 nm

Figure 4.5 also shows the normalized PL spectra of CdSe NCs and CdSe/ZnS NCs grown over them. The red shift that suitable with the one at absorption spectra indicates the growth of ZnS shells over CdSe core NCs.

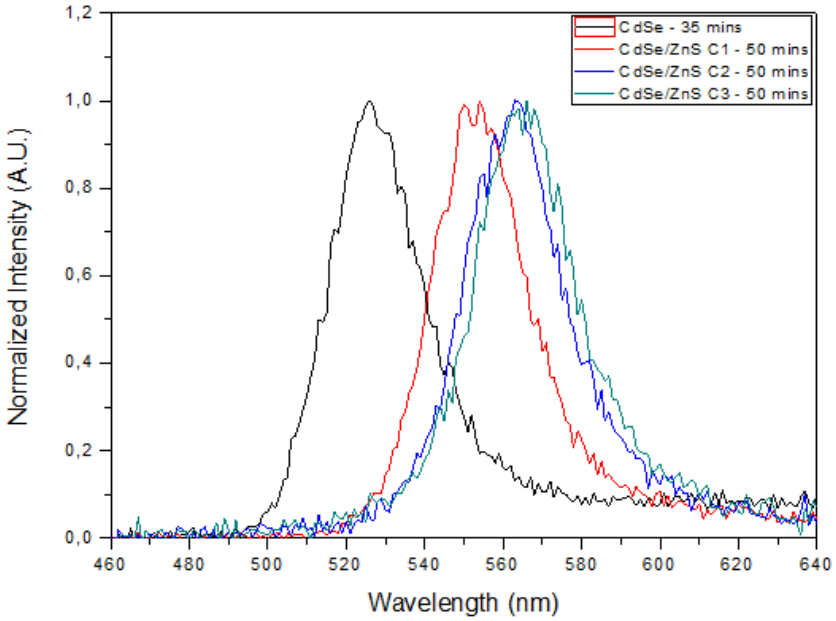

Figure 4.5: Normalized PL spectra of CdSe and CdSe/ZnS NCs.

Table 4.2 and shows the PL properties of CdSe core and CdSe/ZnS core-shell nanostructures for given conditions. A noticable decrease in the PL QY was recorded for second and third cycles of ZnS shell growth process, which is not expected in order to obtain good emission quality by passivating the core surface. In general, a low PL QY is considered as a result of the surface states located in the band gap of the NCs, which act as trapping states for the photogenerated charges. These surface trapping sites are originated from the dangling bonds of some of the surface atoms. The ligands on the surface of NCs may remove some or all of the surface trapping states and increase the PL QY of NCs. Theoretical treatments indicate that the efficiency of the electronic passivation provided by the surface ligands depend strongly on the surface structure and the nature of the surface states of the NCs themselves. If the surface ligands could provide a good electronic passivation for the surface states of the NCs, a high PL QY is expected.

However, decrease in the PL QY for stable conditions can be taken as ordinary, where the most of reports in the literature include the efficiencies of better samples. Chattopadhyay *et al*. (2012) have demonstrated that there is an ideal ratio between the diameter of core and shell thickness for different thicknesses of CdSe core QDs [41]. Normally, the resulting core solution of CdSe NCs was used for the shell growth in the originated article. In this study, the CdSe core QDs for the ZnS shell growth were choosen from the samples with highest PL intensity within each

synthesis and also aliquots were taken for once at constant time intervals to monitor the growth of ZnS shells.

Table 4.2: PL properties of CdSe QDs grown at 160°C with Cd:Se ratio of 1:1.25 and CdSe/ZnS QDs deposited over with number of cycles.

Sample	Cycle Number	Reaction Time	FWHM	Peak Site	QY
CdSe	-	35 mins	27 nm	526 nm	29.18%
CdSe/ZnS	1	50 mins	27.7 nm	553 nm	42.46%
CdSe/ZnS	2	50 mins	28.9 nm	562 nm	21.65%
CdSe/ZnS	3	50 mins	29.5 nm	565 nm	18.38%

Table 4.3 shows the PL properties of CdSe core and CdSe/ZnS core-shell nanocrystals grown on throughout one cycle during the synthesis for given conditions. PL QY reaches its best in early stages of shell coverage process due to small diameter of choosen CdSe nanocrystals.

Table 4.3: PL properties of CdSe QDs grown at 170°C with Cd:Se ratio of 2:1 and CdSe/ZnS QDs deposited over within one cycle for given time intervals.

Sample	Cycle Number	Reaction Time	FWHM	Peak Site	QY
CdSe	-	45 mins	28.3 nm	535 nm	14.49%
CdSe/ZnS	1	10 mins	28.7 nm	542 nm	40.87%
CdSe/ZnS	1	20 mins	29.1 nm	546 nm	24.97%
CdSe/ZnS	1	30 mins	30.3 nm	550 nm	22.31%

Figure 4.6 shows the PL characteristics of choosen CdSe core nanocrystal with small FWHM value, proving narrow particle size distribution.

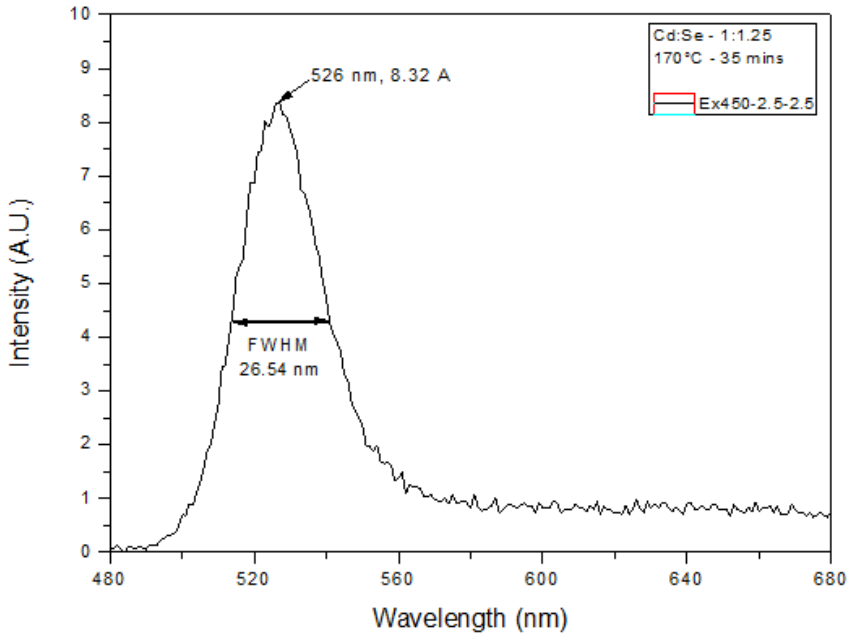

Figure 4.6: PL spectra of CdSe QDs synthesized at 170°C with Cd:Se ratio of 1:1.25.

5. CONCLUSION

Semiconductor CdSe core NCs were synthesized via using collidal chemistry by modifying a published method at moderately lower growth temperatures. ZnS shells were deposited over CdSe core NCs by using a seeding-growth technique throughout the number of cycles. Optical properties of colloidal CdSe and CdSe/ZnS NCs were successfully controlled by changing the initial Cd:Se molar ratios and temperature. Optical absorption and emission spectra both showed gradual red shift with increasing Cd:Se molar ratio and temperature. Additionally, FWHM values obtained from the emission spectras were helped to prove the narrow size distribution, which coincides with the matching results of HRTEM images and theoretical calculations. XRD patterns were showed that both CdSe core and ZnS shell NCs have zinc blende structure.

While the shell material ZnS leads to a suitable electronic passivation due to the large band offsets with respect to CdSe, the CdSe/ZnS core-shell NCs are irregular in shape and the PL QY decreases for large shell thicknesses due to lattice imperfections and number of surface trapping states.

REFERENCES

[1] **Albero, J., Riente, P., Clifford, J. N., Pericàs, M. A., & Palomares, E**. (2013). Improving CdSe Quantum Dot/Polymer Solar Cell Efficiency Through the Covalent Functionalization of Quantum Dots: Implications in the Device Recombination Kinetics. *The Journal of Physical Chemistry C*, ***117*(26)**, 13374-13381.

[2] **Nadarajah, A., Smith, T., & Könenkamp, R**. (2012). Improved Performance of Nanowire–Quantum-Dot–Polymer Solar Cells by Chemical Treatment of the Quantum Dot with Ligand and Solvent Materials. *Nanotechnology*, ***23*(48)**, 485403.

[3] **Kashyout, A. B., Soliman, H. M., Fathy, M., Gomaa, E. A., & Zidan, A. A**. (2012). CdSe Quantum Dots for Solar Cell Devices. *International Journal of Photoenergy* , *2012*, 1-7.

[4] **Li, C., Yang, L., Xiao, J., Wu, Y., Søndergaard, M., Luo, Y., *et al***. (2013). ZnO Nanoparticle Based Highly Efficient CdS/CdSe Quantum Dot-Sensitized Solar Cells. *Physical Chemistry Chemical Physics*, ***15*(22)**, 8710.

[5] **Huang, C., Su, Y., Wen, T., Guo, T., & Tu, M.** (2008). Single-Layered Hybrid DBPPV-CdSe–ZnS Quantum-Dot Light-Emitting Diodes. *IEEE Photonics Technology Letters* , ***20*(4)**, 282-284.

[6] **Shen, C., Li, K., Hou, Q., Feng, H., & Dong, X.** (2010). White LED Based on YAG: Ce, Gd Phosphor and CdSe–ZnS Core/Shell Quantum Dots. *IEEE Photonics Technology Letters* , ***22*(12)**, 884-886.

[7] **Chen, M., Yang, J., & Shiojiri, M.** (2012). ZnO-Based Ultra-Violet Light Emitting Diodes and Nanostructures Fabricated by Atomic Layer deposition. *Semiconductor Science and Technology*, ***27*(7)**, 074005.

[8] **Deng, L., Han, L., Xi, Y., Li, X., & Huang, W.** (2012). Design Optimization for High-Performance Self-Assembled Quantum Dot Lasers With Fabry–Perot Cavity. *IEEE Photonics Journal*, ***4*(5)**, 1600-1609.

[9] **Yan, J. H., Wang, C. G., Zhang, H., & Cheng, C.** (2012). Evaluation of Emission Cross Section of CdSe Quantum Dots for Laser Applications. *Laser Physics Letters*, ***9*(7)**, 529-531.

[10] **Peng, X., Wickham, J., & Alivisatos, A. P.** (1998). Kinetics of II-VI and III-V Colloidal Semiconductor Nanocrystal Growth: "Focusing" of Size Distributions. *Journal of the American Chemical Society*, ***120*(21)**, 5343-5344.

[11] **Mi, W., Tian, J., Jia, J., Tian, W., Dai, J., & Wang, X.** (2012). Characterization of Nucleation and Growth Kinetics of the Formation of Water-Soluble CdSe Quantum Dots by Their Optical Properties. *Journal of Physics D: Applied Physics*, ***45*(43)**, 435303.

[12] **Peter, A. J., & Lee, C. W.** (2012). Electronic and Optical Properties of CdS/CdZnS Nanocrystals. *Chinese Physics B*, ***21*(8)**, 087302.

[13] **Buckley, S., Rivoire, K., & Vučković, J.** (2012). Engineered Quantum Dot Single-Photon Sources. *Reports on Progress in Physics*, ***75*(12)**, 126503.

[14] **Hu, L., Wu, H., Wan, Z., Cai, C., Xu, T., Lou, T., *et al.*** (2012). Physical Approaches to Tuning the Luminescence Color Patterns of Colloidal Quantum Dots. *New Journal of Physics*, ***14*(1)**, 013059.

[15] **Shu, G., Lee, W., Shu, I., Shen, J., Lin, J., Chang, W., *et al.*** (2005). Photoluminescence of Colloidal CdSe/ZnS Quantum Dots Under Oxygen Atmosphere. *IEEE Transactıons On Nanotechnology*, ***4*(5)**, 632-636.

[16] **Zhu, H., Prakash, A., Benoit, D. N., Jones, C. J., & Colvin, V. L.** (2010). Low Temperature Synthesis of ZnS and CdZnS Shells on CdSe Quantum Dots. *Nanotechnology*, ***21*(25)**, 255604

[17] **Xie, R., Kolb, U., Li, J., Basche, T., & Mews, A.** (2005). Synthesis and Characterization of Highly Luminescent CdSe-Core CdS/Zn0.5Cd0.5S/ZnS Multishell Nanocrystals.. *ChemInform*, ***36*(36)**, 7480-7488.

[18] **Shen, H., Yuan, H., Niu, J. Z., Xu, S., Zhou, C., Ma, L., *et al*.** (2011). Phosphine-Free Synthesis of High-Quality Reverse Type-I ZnSe/CdSe Core with CdS/CdZnS/ZnS Multishell Nanocrystals and Their Application for Detection of Human Hepatitis B Surface Antigen. *Nanotechnology*, ***22*(37)**, 375602.

[19] **Luong, B. T., Hyeong, E., Ji, S., & Kim, N.** (2012). Green Synthesis of Highly UV-Orange Emitting ZnSe/ZnS:Mn/ZnS Core/Shell/Shell Nanocrystals by a Three-Step Single Flask Method. *RSC Advances* , ***2*(32)**, 12132.

[20] **Sattler, K. D.** (2011). Chapter 35: Core-Shell Quantum Dots. *Handbook of Nanophysics* (pp. 35-4-35-5). Boca Raton: CRC Press/Taylor & Francis.

[21] **Fonoberov, V. A., & Balandin, A. A.** (2003). Excitonic Properties of Strained Wurtzite and Zinc-Blende GaN/Al[sub x]Ga[sub 1−x]N Quantum Dots. *Journal of Applied Physics*, ***94*(11)**, 7178.

[22] **Efros, Al. L.** (1982). Interband Absorption of Light in a Semiconductor Sphere. *Soviet Physics Semiconductors*, ***16*(7)**, 772-775.

[23] **Mccumber, D.** (1964). Einstein Relations Connecting Broadband Emission and Absorption Spectra. *Physical Review*, ***136*(4A)**, A954-A957.

[24] **Peng, Z. A., & Peng, X.** (2001). Formation of High-Quality CdTe, CdSe, and CdS Nanocrystals Using CdO as Precursor. *Journal of the American Chemical Society*, ***123*(1)**, 183-184.

[25] **Talapin, D. V., Rogach, A. L., Kornowski, A., Haase, M., & Weller, H.** (2001). Highly Luminescent Monodisperse CdSe and CdSe/ZnS Nanocrystals Synthesized in a Hexadecylamine−Trioctylphosphine Oxide−Trioctylphospine Mixture. *Nano Letters*, ***1*(4)**, 207-211.

[26] **Wang, Y. A., Li, J. J., Chen, H., & Peng, X.** (2002). Stabilization of Inorganic Nanocrystals by Organic Dendrons. *Journal of the American Chemical Society*, ***124*****(10)**, 2293-2298.

[27] **Donegá, C. D., Hickey, S. G., Wuister, S. F., Vanmaekelbergh, D., & Meijerink, A.** (2003). Single-Step Synthesis to Control the Photoluminescence Quantum Yield and Size Dispersion of CdSe Nanocrystals. *The Journal of Physical Chemistry B*, ***107*****(2)**, 489-496.

[28] **Jun, S., Jang, E., & Lim, J. E.** (2006). Synthesis of Multi-Shell Nanocrystals by a Single Step Coating Process. *Nanotechnology*, ***17*****(15)**, 3892-3896.

[29] **Pan, D., Wang, Q., Jiang, S., Ji, X., & An, L.** (2007). Low-Temperature Synthesis of Oil-Soluble CdSe, CdS, and CdSe/CdS Core-Shell Nanocrystals by Using Various Water-Soluble Anion Precursors. *Journal of Physical Chemistry C*, ***111*****(15)**, 5661-5666.

[30] **Kaur, G., & Tripathi, S.** (2014). Size Tuning of MAA Capped CdSe and CdSe/CdS Quantum Dots and Their Stability in Different pH Environments. *Materials Chemistry and Physics*, ***143*****(2)**, 514-523.

[31] **Zhu, C., Wang, P., Wang, X., & Li, Y.** (2008). Facile Phosphine-Free Synthesis of CdSe/ZnS Core/Shell Nanocrystals Without Precursor Injection. *Nanoscale Research Letters*, ***3*****(6)**, 213-220.

[32] **Tian, C., Wang, E., Kang, Z., Mao, B., Zhang, C., Lan, Y., *et al.*** (2006). Synthesis of Ag-Coated Polystyrene Colloids by an Improved Surface Seeding and Shell Growth Technique. *Journal of Solid State Chemistry*, ***179*****(11)**, 3270-3276.

[33] **Murray, C. B., Norris, D. J., & Bawendi, M. G.** (1993). Synthesis and Characterization of Nearly Monodisperse CdE (E = Sulfur, Selenium, Tellurium) Semiconductor Nanocrystallites. *Journal of the American Chemical Society*, ***115*****(19)**, 8706-8715.

[34] **Xing, Y., Wang, M. D., Chaudry, Q., Nie, S., Simons, J. W., Yezhelyev, M. V., *et al.*** (2007). Bioconjugated Quantum Dots for Multiplexed and Quantitative Immunohistochemistry. *Nature protocols*, ***2*****(5)**, 1152-1165.

[35] **Yang, C., Xie, H., Li, Y., Zhang, J., & Su, B.** (2013). Direct and Rapid Quantum Dots Labelling of Escherichia Coli Cells. *Journal of Colloid and Interface Science*, ***393***, 438-444.

[36] **Hines, M. A., & Guyot-Sionnest, P.** (1996). Synthesis and Characterization of Strongly Luminescing ZnS-Capped CdSe Nanocrystals. *The Journal of Physical Chemistry*, ***100*****(2)**, 468-471.

[37] **Qu, L., & Peng, X.** (2002). Control of Photoluminescence Properties of CdSe Nanocrystals in Growth. *Journal of the American Chemical Society*, ***124*****(9)**, 2049-2055.

[38] **Talapin, D. V., Rogach, A. L., Shevchenko, E. V., Kornowski, A., Haase, M., & Weller, H.** (2002). Dynamic Distribution of Growth Rates within the Ensembles of Colloidal II−VI and III−V Semiconductor Nanocrystals as a Factor Governing Their Photoluminescence Efficiency. *Journal of the American Chemical Society*, ***124*****(20)**, 5782-5790.

[39] **Grabolle, M., Spieles, M., Lesnyak, V., Gaponik, N., Eychmüller, A., & Resch-Genger, U.** (2009). Determination of the Fluorescence Quantum Yield of Quantum Dots: Suitable Procedures and Achievable Uncertainties. *Analytical Chemistry*, ***81*****(15)**, 6285-6294.

[40] **Bhattacharjee, B., Hsu, C., Lu, C., & Chang, W. H.** (2006). Colloidal CdSe–ZnS Core-Shell Nanoparticles: Dependence of Physical Properties on Initial Cd to Se Concentration. *Physica E: Low-dimensional Systems and Nanostructures*, ***33*****(2)**, 388-393.

[41] **Chattopadhyay, S., Sen, P., Andrews, J. T., & Sen, P. K.** (2012). Effect of Shell and Shell Thickness on Photoluminescence (PL) of a CdSe/ZnS Core – Shell Quantum Dot. *Journal of Physics: Conference Series*, ***365***, 012037.

CURRICULUM VITAE

Name Surname:	Hakan AYDIN
Place and Date of Birth:	Istanbul, 28/09/1988
Address:	İTÜ Ayazağa Campus, Faculty of Arts & Sciences, Department of Physics Engineering, NANOSEM Semiconductor Research Labrotary – 34469 Maslak-İstanbul
E-Mail:	haydin@itu.edu.tr
B.Sc.:	Yıldız Technical University / Department of Physics

PUBLICATIONS/PRESENTATIONS ON THE THESIS

- **Aydın H.,** Karim M. R., Balaban M. & Ünlü H. (2014). Colloidal Synthesis and Characterization of CdSe Quantum Dots (QDs): Role of Cd:Se Molar Ratio and Temperature. *30th Europan Conference on Surface Science (ECOSS-30).* (Accepted)